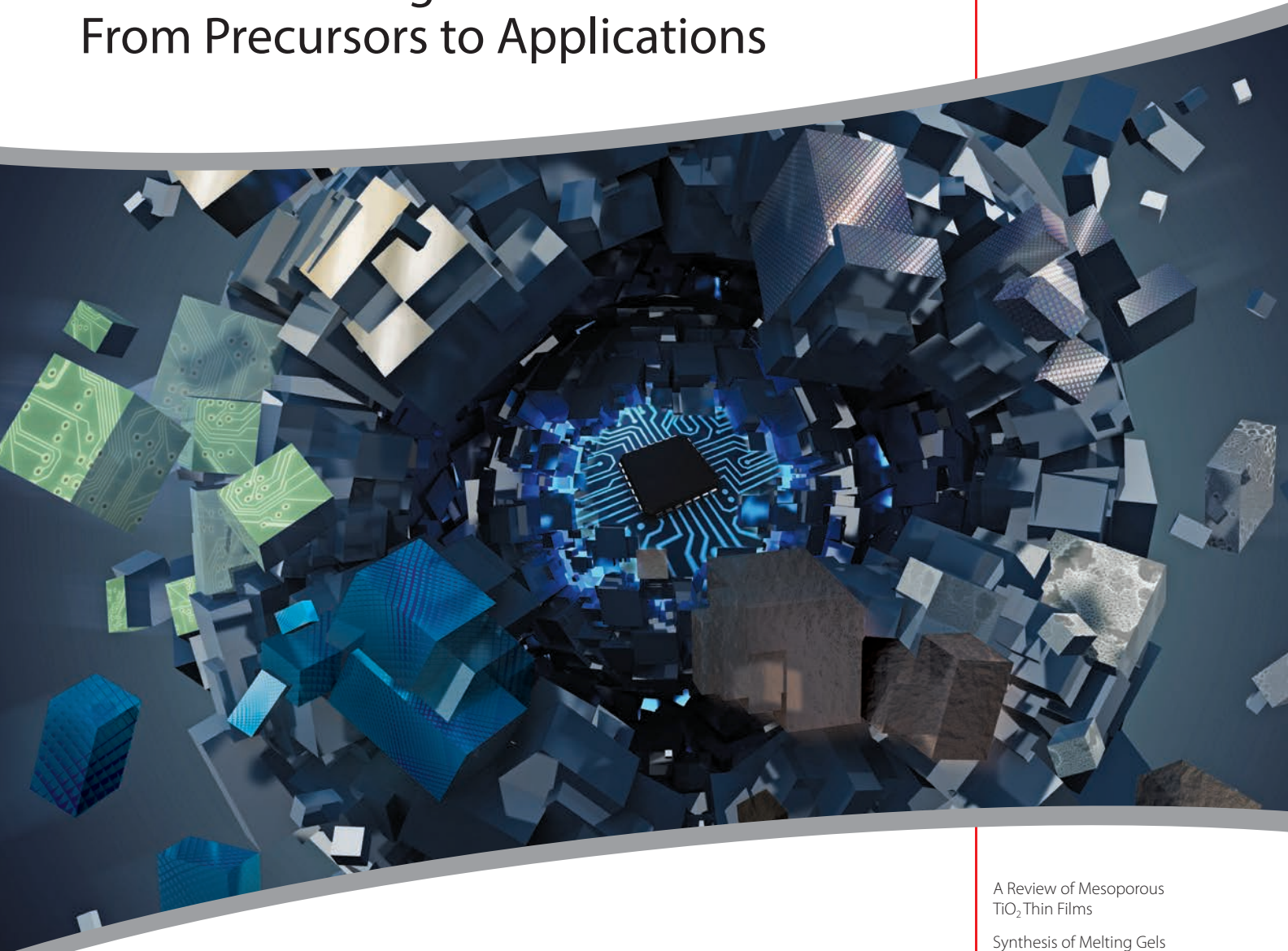


Material Matters™

Volume 7, Number 2

ALDRICH
Materials Science

Functional Inorganic Materials: From Precursors to Applications



Building Up for Tomorrow

A Review of Mesoporous
TiO₂ Thin Films

Synthesis of Melting Gels
Using Mono-Substituted and
Di-Substituted Alkoxy-siloxanes

Nanostructured Materials Through
Ultrasonic Spray Pyrolysis

Advanced Inorganic Materials for
Solid State Lighting

SIGMA-ALDRICH®



Introduction

Welcome to the second issue of *Material Matters*™ for 2012 focusing on Functional Inorganic Materials: From Precursors to Applications.

Functional inorganic materials can be broadly defined as materials which can exhibit specific properties critical for end applications. This special class of materials has emerged to play a profound role in modern technologies and find use in numerous applications such as microelectronics, computer memories, coatings, optics, sensors, catalysis, photovoltaics, energy storage and biomedicine. Rapidly changing technologies continue to drive the discovery of new materials. Recent advances in the area of functional materials include the development of porous materials, light-emitting materials, thermoelectric materials, ionic and electronic conducting materials, and nanomaterials.

Crucial to these advances is understanding the relationships between composition, structure, and properties of these newly-developed functional materials, along with the dependence of their properties on precursors and processing methods. The preparation of materials in a scalable and continuous manner is another key requirement for the transition of new materials to the market. Soft chemistry or "*chimie douce*" has shown great success in fabricating functional and nanostructured materials with the possibility to control the reaction pathways during the transformation of the precursor species to the final product. Among the various "soft" chemistry routes, sol-gel based procedures proved to be particularly successful in the preparation of various "hard and soft" functional materials.

The current issue of *Material Matters*™ features articles that highlight the preparation of functional inorganic materials synthesized by sol-gel and related techniques, and their applications. To begin with Prof. Jinshu Wang (Beijing University of Technology, Beijing, China) reviews the preparation of mesoporous titanium dioxide thin films by hard and soft templating processes and its application in semiconductor photocatalysis. In the second article, Prof. Lisa Klein (Rutgers University, USA) and Prof. Andrei Jitianu (City University of New York, USA) describe a new type of inorganic-organic hybrid material called melting gels, the effect of the nature of the precursors on the properties of the melting gels and their applications as "low κ " dielectric materials in integrated circuits for metal-oxide semiconductor field effect transistors. In the next article, Prof. Kenneth Suslick from University of Illinois at Urbana-Champaign, USA highlights the diversity of applications of different types of nanostructured materials and their preparation in a very scalable and continuous manner using ultrasonic spray method. In the last article, Prof. Ram Seshadri (University of California at Santa Barbara, USA) presents the state-of-the-art in solid state lighting and describes the use of oxides, oxynitrides and nitrides doped with small amounts of rare earth and/or transition metal elements to efficiently create white light in a solid-state device.

Each article in this publication is accompanied by a list of relevant materials available from Aldrich Materials Science. For additional product information, please visit Aldrich Materials Science at aldrich.com/matsci. Please send us your comments or suggestions for *Material Matters*™ or your product suggestions at matsci@sial.com.

About Our Cover

The development of novel inorganic materials with specific functionalities is a major focus of today's materials science research. With a rapidly-evolving technological climate, the significance of these functional materials will only increase in the future. The cover art of this issue reflects this significance by illustrating the conversion of inorganic precursors into an advanced, functional material with applications in high-tech industries including microelectronics, semiconductors, smart coatings and alternative energy.



Meenakshi Hardi, Ph.D.
Aldrich Materials Science
Sigma-Aldrich Corporation

Material Matters™

Vol. 7, No. 2

Aldrich Materials Science
Sigma-Aldrich Co. LLC
6000 N. Teutonia Ave.
Milwaukee, WI 53209, USA

To Place Orders

Telephone 800-325-3010 (USA)
FAX 800-325-5052 (USA)

Customer & Technical Services

Customer Inquiries 800-325-3010
Technical Service 800-231-8327
SAFC® 800-244-1173
Custom Synthesis 800-244-1173
Flavors & Fragrances 800-227-4563
International 414-438-3850
24-Hour Emergency 414-438-3850
Website sigma-aldrich.com
Email aldrich@sial.com

Subscriptions

To request your **FREE** subscription to *Material Matters*, please contact us by:

Phone: 800-325-3010 (USA)
Mail: Attn: Marketing Communications
Aldrich Chemical Co., Inc.
Sigma-Aldrich Co. LLC
P.O. Box 2988
Milwaukee, WI 53201-2988
Website: aldrich.com/mm
Email: sams-usa@sial.com

International customers, please contact your local Sigma-Aldrich office. For worldwide contact information, please see last page.

Material Matters is also available at aldrich.com/matsci.

Aldrich brand products are sold through Sigma-Aldrich Co. LLC. Purchaser must determine the suitability of the product for its particular use. See product information on the Sigma-Aldrich website at sigma-aldrich.com and/or on the reverse side of invoice or packing slip for additional terms and conditions of sale.

All prices are subject to change without notice.

Material Matters (ISSN 1933-9631) is a publication of Aldrich Chemical Co., Inc. Aldrich is a member of the Sigma-Aldrich Group. © 2012 Sigma-Aldrich Co. LLC.

Your Materials Matter



Shashi Jasty

Shashi G. Jasty, Ph.D.
Director, Aldrich Materials Science

Prof. Mikhail Fedorov of Ioffe Physical-Technical Institute, St. Petersburg, Russia, kindly suggested that we offer high purity Magnesium Silicide (Aldrich Prod. No. 752630) as a material for thermoelectric applications. Mg_2Si is a very valuable thermoelectric material due to its low toxicity, high thermal stability, electronic transport properties and relative abundance of magnesium and silicon.¹⁻³ Low levels of metal impurities are essential for reproducible thermoelectric characteristics of the material.^{3,4}

Other applications of magnesium silicide include semiconducting layers with high absorption coefficients for solar cells and anode materials for lithium ion batteries.^{5,6}

References

- (1) Fedorov, M. I.; Zaitsev, V. K. *Material Matters* 2011, 4, 100.
- (2) Valset, K.; Flage-Larsen, E.; Stadelmann, P.; Taftø, J. *Acta Materialia* 2012, 60(3), 972.
- (3) Boulet, P.; Record, M.-C. *J. Chem. Phys.* 2011, 135(23), 234702/1.
- (4) Sakamoto, T.; Iida, T.; Fukushima, N.; Honda, Y.; Tada, M.; Taguchi, Y.; Mito, Y.; Taguchi, H.; Takahashi, Y. *Thin Solid Films* 2011, 519(24), 8528.
- (5) Takashi, K.; Yuichiro, S.; Hiroyuki, F. *J. Appl. Phys.* 2011, 110, 063723.
- (6) Imai, Y.; Watanabe, A. *J. Alloys Compd.* 2011, 509(30), 7877.

We welcome fresh product ideas from you. Do you have a material or compound you wish to see in our Aldrich Materials Science line? If it is needed to accelerate your research, it matters. Send your suggestion to matsci@sial.com for consideration.



Magnesium silicide

Dimagnesium silicide [22831-39-6]
 Mg_2Si FW 76.70

Mg_2Si

► pieces, 99.7% trace metals basis

752630-5G

5 g

New Feature

Explore previous editions of *Material Matters* by scanning the QR code below.



or visit

aldrich.com/materialmatters

Table of Contents

Articles

A Review of Mesoporous TiO_2 Thin Films	2
Synthesis of Melting Gels Using Mono-Substituted and Di-Substituted Alkoxysiloxanes	8
Nanostructured Materials through Ultrasonic Spray Pyrolysis	15
Advanced Inorganic Materials for Solid State Lighting	22

Featured Products

Titanium Precursors: Alkoxides and Halogenides (A selection of sol-gel precursors of titanium)	5	Silicon Precursors for Hybrid and Melting Gels: Silylamines and Silazanes (A selection of nitrogen containing silicon precursors)	13
Titanium Precursors: Thin Film Deposition (A list of vapor deposition precursors of titanium)	6	Wafers and Substrates (A list of substrates for deposition of melting gels)	14
Titanium Oxide Nanomaterials (A selection of titanium oxide nanopowders and nanoparticle dispersions)	6	Quantum Dots (CdS and CdSe based quantum dots of different particle size and quantum yields)	19
Silicon Precursors for Hybrid and Melting Gels: Silicates and Siloxanes (Silicates, mono-, di- and tri-substituted alkoxysiloxanes for sol-gel synthesis)	11	Nanoparticles and Inks (Au and Ag nanoparticles and inks for printed circuits and biomedical applications)	19
Silicon Precursors for Hybrid and Melting Gels: Silanes (A selection of alkyl and phenyl silanes and disilanes)	12	Common Precursors for Ultrasonic Spray Pyrolysis (Metal salts, acetates, carbonyls and alkoxides for synthesis of nanostructured materials)	19
Silicon Precursors for Hybrid and Melting Gels: Chlorosilanes and Halogenides (High purity chlorosilanes and silicon halogenides for sol-gel synthesis)	13	Precursors for Phosphor Materials (Metal precursors for inorganic phosphor host and dopant materials)	26



A Review of Mesoporous TiO₂ Thin Films



Jinshu Wang*, Junshu Wu, Hongyi Li
The Key Lab of Advanced Functional Materials, Ministry of Education China,
School of Materials Science and Engineering, Beijing University of Technology,
Beijing 100124, China
*Email: wangjsh@bjut.edu.cn

Introduction

Titanium dioxide (TiO₂) is an important *n*-type semiconducting material that shows interesting characteristics such as photoswitchable surface wettability, high photocatalytic activity, bistable electrical resistance states and high electron drift mobility. The photocatalytic activity, strong oxidizing properties and photoresponsive behavior of titania find applications as antifogging, self cleaning and disinfecting coatings on medical devices, food preparation surfaces and building materials. Titanium dioxide is the most widely used white pigment because of its brightness and very high refractive index and is found in all kinds of paints, printing ink, plastics, paper, synthetic fibers, ceramics, electronic components along with food and cosmetics. Among the many TiO₂-based materials with distinct structural and geometrical features, mesoporous TiO₂ architectures represent an important class of novel materials which have recently attracted a renewed interest in both fundamental and applied materials research.¹⁻⁴ Hard and soft-templating syntheses are the two most widely used methods to prepare this class of porous materials.

The hard-template assisted route involves the use of colloidal particles, for example, polymeric beads, and anodic alumina membranes. The nanostructures are formed on the inner or outer surfaces of the templates using sol-gel casting or other particle adsorption methods. Removal of these templates then generates these unique porous materials.

The soft-template assisted route involves the use of ionic organic surfactants or nonionic polymeric surfactants which self-assemble into a diversity of supermolecular structures including, spherical micelles, hexagonal rods, lamellar liquid crystals and other assemblies in solution, driven by non-covalent weak interactions such as hydrogen bonding, van der Waals forces and electrostatic interaction between the surfactants and the building blocks. These assemblies are then used as soft templates to tune the pore structure and size of porous materials.

In this paper, we discuss recent advances in the preparation of various TiO₂ porous structures via hard and soft-templating routes. Specifically, we focus on recent developments in TiO₂ mesoporous thin films in a combined sol-gel and evaporation-induced self-assembly (EISA) process.

Hard-Templating Syntheses of TiO₂ Porous Structures

Hard-templating is the most commonly used approach for the preparation of TiO₂ porous materials over the past two decades.^{5,6} Porous inorganic materials are found in the natural world. Such structures, with periodic pores, are remarkable for their morphological and crystallographic control. They can be used to fabricate ordered three-dimensional (3D) TiO₂ porous structures with a crystalline framework, high specific surface area and tailored pore structure through controlled nucleation and templating.

Sandhage et al. demonstrated that an intricate, 3D, nanocrystalline rutile TiO₂ (Aldrich Prod. Nos. 635065, 637262, 204730) structure was generated with the morphology and nanoscale features inherited from a chitin-based *Morpho* butterfly wing template.⁷ In order to obtain hierarchical TiO₂ porous structures with the synergistic advantages of mesoporous and macroscale morphologies, Moon et al. introduced a method to engineer hierarchical TiO₂ materials consisting of meso and macroscale pores using a dual templating method.⁸ Monodisperse polystyrene (PS) colloidal particles were injected into the template. After coating with TiCl₄ (Aldrich Prod. Nos. 254312, 208566) solution, both the holographic and colloidal dual templates were calcined in an air environment. This resulted in anatase TiO₂ structures with macropores (250 nm in diameter) due to the removal of the holographic patterns. It also resulted in mesoscale pores (50 nm in diameter) due to the removal of the PS particles.

Buschbaum et al. prepared hierarchically mesoporous sponge-like structure TiO₂ films with partially interconnected pores of a circular shape and with a diameter of about 30-40 nm. They did this by combining poly(methyl methacrylate) (Aldrich Prod. Nos. 445746, 182265, 182230), PMMA microsphere secondary templating and sol-gel chemistry with an amphiphilic diblock copolymer (PDMS-*b*-MA(PEO)) as a structure-directing agent (Figure 1A).⁹ A phase separation in an amphiphilic block copolymer was induced in this approach, while the Ti precursor was chemically linked to one of the blocks. The structure in the sol-gel solution was transferred to solid thin films with TiO₂ particles embedded in microspheres.

With increasing PMMA microsphere addition, the number of surface depressions created in the films increased, together with the tendency for agglomeration. Additionally, the size of the mesopores was decreased (Figure 1B, C). This was attributed to the complex interplay of all the components involved in the sol-gel process by the addition of a second templating polymer. This influenced the phase separation in existing primary structures. The mesopore size can be further decreased by selecting a decent block copolymer as a structure-directing agent. By using amphiphilic triblock copolymer Pluronic® P123 (EO₂₀PO₇₀EO₂₀) combined with a hard templating process, Xu et al. synthesized ordered arrays of mesoporous titania spheres with mesopore size in the range of ~35 nm.¹⁰ The titania precursor solution containing EO₂₀PO₇₀EO₂₀ was infiltrated into the spherical macropores of the PMMA mesh which was prepared by using silica opal. Ordered mesoporous TiO₂ sphere arrays were finally obtained by removing the PMMA mesh template and the triblock copolymer surfactant. However, the elimination of solid hard-templates increases the cost and risk of large-scale manufacture, and thus lots of challenges are left to scientists in the discipline domains.

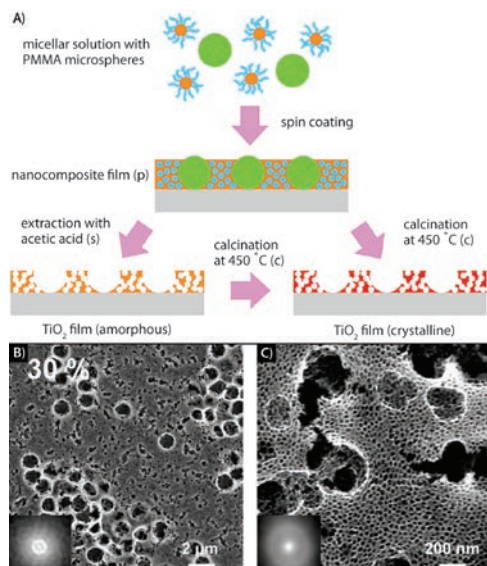


Figure 1. A) Illustration of the preparation route for hierarchical structuring of TiO₂. B, C) SEM images of TiO₂ films with 30% amounts of PMMA microspheres added to the sol-gel solution.⁹ Reprinted with permission from Kaune, G; et al. *Applied Materials* **2009**, 1(12), 2862-2869. Copyright 2009 American Chemical Society.

Soft-Templating Syntheses of TiO₂ Porous Structures

EISA offers excellent opportunities for the reproducible synthesis of mesoporous metal oxide films. The self-assembly of block copolymer, driven by evaporation, offers an excellent opportunity in directing mesostructures for inorganic species. Selection of appropriate starting materials, especially the Ti source and block copolymer, is vital in the successful preparation of highly organized mesoporous structure of TiO₂ films. The suitable Ti source is quite limited. Available titanium alkoxides include titanium ethoxide (Ti(OEt)₄) (Aldrich Prod. No. 244759), titanium isopropoxide (Ti(O-iPr)₄) (Aldrich Prod. No. 687502), and titanium butoxide (Ti(OBu)₄) (Aldrich Prod. No. 244112), listed in an order of increasing reactivity in hydrolysis. Compared with other Ti sources such as TiF₄ (Aldrich Prod. No. 333239), they show predominant performances in controlling the homogeneity of the initial solution and final size of TiO₂ crystallites on the nanoscale.¹¹

The ideal block copolymers for EISA are molecules with a polar hydrophilic head which is attracted to water and a hydrophobic hydrocarbon chain which is attracted to oil. In water, the hydrocarbon chains tend to self-associate to minimize contact with the water molecules, leading to the formation of various aggregates. Organized soft-template systems such as micelles, reverse micelles, vesicles, liquid droplets, etc. have been widely exploited to provide effective routes to grow porous structures.^{12,13}

For the suitable block copolymers, commercially-available amphiphilic poly(ethylene oxide)-block-poly(propylene oxide)-block-poly(ethylene oxide) (PEO-PPO-PEO) triblock copolymers, typically Pluronic® P123 (PEO₂₀PPO₇₀PEO₂₀, EO = ethylene oxide, PO = propylene oxide, M_w = 5800) (Aldrich Product No. 435465) and F127 (PEO₁₀₆PPO₇₀PEO₁₀₆, M_w = 12,600) (Sigma Prod. No. P2443), consisting of a central hydrophobic PPO chain and two hydrophilic PEO tails, have been widely used as the structure-directing agents for the construction of highly organized mesoporous structures for TiO₂, where P and F stand for the physical forms of paste and flake, respectively.¹⁴

Rankin et al. combined P123 surfactant templating and polypropylene glycol (PPG) (Aldrich Prod. Nos. 202304, 202355, 81380) phase separation to generate hierarchically porous titania thin films.¹⁵ As shown in Figure 2A, PPG behaved as a hydrophilic compound and was incorporated into the polar titanate-rich phase at the initial low-temperature period. However, during high-temperature drying, PPG switched to being hydrophobic and drove the phase separation process, either due to a change in the entropic driving force during polymerization of the titanate species or the enthalpic driving force associated with PPG interactions with other species. A high mass ratio of PPG to P123 (M = 0.3) induced uniform mesopores with a high degree of long-range order and hexagonal symmetry (Figure 2B-D).

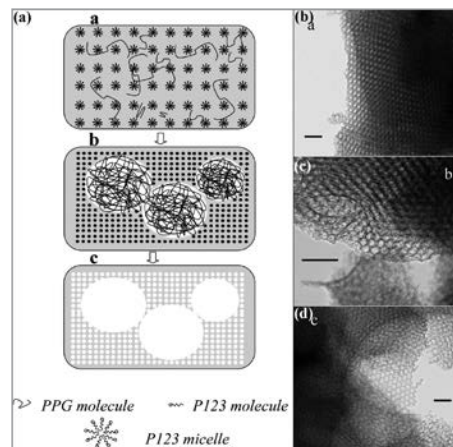


Figure 2. A) Formation mechanism of thin films with hierarchical porous architecture. B-D) High-magnification TEM images of calcined TiO₂ thin films prepared with mass ratios of PPG to P123 (M) = B) 0.3, C) 0.5, or D) 1. Scale bar = 50 nm.¹⁵ Reprinted with permission from Wu, Q; et al. *Langmuir* **2011**, 27(15), 9557-9566. Copyright 2011 American Chemical Society.

In our group^{16,17}, we prepared high-quality mesoporous titania thin films with good thermal stability (up to 600 °C) by using triblock copolymer Pluronic® F127 as the structure-directing agent and tetrabutyl titanate as the inorganic precursor. The excellent thermal stability is correlated to the thick wall of the mesostructure.

The use of F127 as the templating agent was the premise for the formation of the thick walls and larger pore diameters in the mesostructure. The F127 was a unique surfactant owing to its high molecular weight with long hydrophilic PEO and hydrophobic PPO segments. This offered the possibility of the formation of thicker walls and larger pore diameters in the mesostructure.

The block copolymer micelle was composed of a core dominated by PPO and a corona dominated by PEO segments. The core of the micelles was believed to be free of water, while the corona was hydrated. The pore size was, to a large extent, dependent on the effective volume of the hydrophobic core (PPO) of the micelles. The wall thickness was determined mainly by the hydrophilic corona (PEO).

In addition, the use of a non-aqueous solvent and Ti(OBu)₄ as the inorganic precursor was very important. During the synthesis of sol, the strong chelating agent, acetylacetonone (Aldrich Prod. No. 10916) and acid solvent, permitted control of the reactivity by avoiding fast hydrolysis and condensation of the precursor in solution. Furthermore, anhydrous solvent depressed the reactivity of the precursor. Under the “dry conditions”, the slow hydrolysis and condensation speed of the inorganic precursor preferred the formation of oligomeric Ti-oxo species or titania clusters. This was the premise for the formation of thick and solid inorganic walls in the framework. These small entities associate preferentially with polyethylene oxide (PEO) (Aldrich Prod. Nos. 372773, 372781, 372838) moieties in the self-assembly process.

Figure 3 shows the transmission electron micrographs of the TiO₂ thin films. Figure 3(A) revealed that the film could maintain homogeneous and well-ordered mesostructure even after calcination at temperature of 600 °C. The mesopores of the film presented with an elliptical shape because of the growth of the crystalline grains. HRTEM image of the film (Figure 3B) showed that the film was composed of high-crystalline nanoparticles. The pore size and wall thickness of the mesostructure were in the range between 6-9 and 9-12 nm, respectively. The ultra thick and robust walls resulted in the good thermal stability of the obtained film. A selected-area electron diffraction (SAED) pattern (inset Figure 3B) of the sample confirmed that these crystallites were anatase.

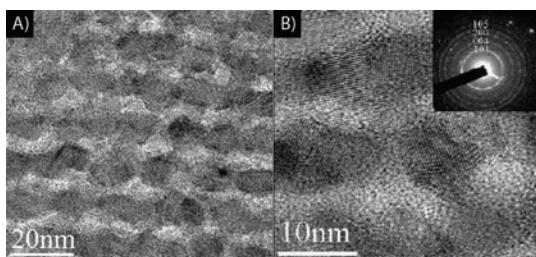


Figure 3. A) TEM image and B) HRTEM image of the synthesized mesoporous TiO₂ thin films prepared with F127 calcined at 600 °C; The inset of Figure 2B is the SAED pattern of the calcined sample.

We also found that the kinds of block copolymer and ions used had a great impact on the thermal stability of TiO₂ films. Figure 4 shows the scanning electron micrographs of the films prepared with different block copolymers and prepared with thiourea ethanol solution, using F127 as the block copolymer. As shown in Figure 4A and B, after calcination at 500 °C, the films prepared with P123 and Brij®58 (EO₂₀CH₁₆H) (Sigma Prod. No. P5884) had low quality mesoporous structure, i.e., some mesoporous structures had deformed and collapsed, whereas those prepared with F127 had exhibited a uniform pore size distribution (Figure 4C). This indicates that the block copolymers which had long hydrophilic PEO and hydrophobic PPO segments were favorable for the formation of thick wall structures. However, when 2.5% (mol) thiourea (Sigma-Aldrich Prod. Nos. T8656, T7875) was added to the solution, the films that were confirmed by the doping of N and S partly lost the uniform mesoporous structure, with some particles on the surface of the film (Figure 4D).

The hydrolysis of the Ti-alkoxide precursors in the acidic solution would result in the formation of nanometer sized Ti-oxo clusters.¹⁸ These were preferentially associated with the hydrophilic PEO block of F127 micelles which formed the hybrid amorphous mesostructure. When thiourea was added to the acidic solution, thiourea might have a chemical reaction with water absorbed from the air to form H₂S and NH₃. The H₂S and NH₃ produced can then react with oxygen in the air and hydrochloric acid to produce sulfur and ammonium chloride.

The excess amount of NH₄Cl (Aldrich Prod. Nos. 254134, 326372) caused the collapse of the mesoporous microstructure since NH₄⁺ of NH₄Cl adsorbed at the micellar interface and changed the micellar curvature. The hydrophilic poly(ethylene oxide) (PEO) blocks became gradually more dehydrated. This increased the effective size of the hydrophobic core at the expense of the hydrophilic corona, leading to the change of the micelle shape from spherical to columnar. As a result, the micelles were difficult to assemble with inorganic-oxo species, leading to the loss of the mesoporous structure.

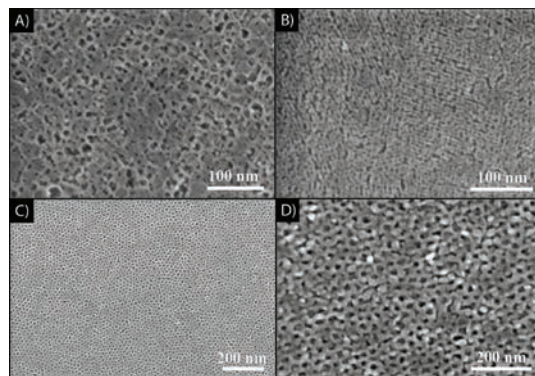


Figure 4. SEM images of the TiO₂ thin films prepared with A) P123, B) Brij58, C) F127 and (D) F127 together with thiourea followed by 500 °C calcinations.

Application of Mesoporous TiO₂

Porous solids possessing large specific surfaces and easily accessible cavities have found wide applications in heterogeneous catalysis, sorption, separation, gas sensing, optoelectronics, host-guest chemistry molecular electronic devices. In this article, we mainly introduced the application of mesoporous TiO₂ into the photocatalysis field. Semiconductor photocatalysis is an established, significant and still-expanding area of research which has led to numerous commercial products, such as self-cleaning glass, tiles and paint.

The current commercial manifestations of photocatalysis usually utilize a layer of the semiconductor photocatalyst, invariably anatase titania (Aldrich Prod. No. 637254, 232033, 248576).¹⁹ The photocatalytic mechanism for the semiconductor is that, upon excitation, a conduction-band electron and a valence-band hole separate. The hole then initiates an oxidative reaction while the electron initiates a reductive reaction. Thus, organic compounds coming in contact with TiO₂ films can be destroyed either through direct oxidation by the trapped holes or attack by hydroxyl groups.

Methods adopted for assessing and characterizing the activities of TiO₂ films include: (i) the discoloration of dyes, such as methylene blue (MB) and methyl orange (MO) dissolved in aqueous solution; (ii) the photomineralization of a thin solid film of a wax-like substance, such as stearic or palmitic acid and (iii) the photo-oxidation of gas phase pollutants.

In our work, we evaluated the photocatalytic activity of mesoporous TiO₂ by photodegradation of methyl orange solution. Figure 5 shows the decomposition of MO aqueous solution of pure mesoporous TiO₂ and N, S doped mesoporous TiO₂ prepared with thiourea under UV illumination. As shown in Figure 5, compared with the standard sample P25, both pure mesoporous TiO₂ and N, S doped TiO₂ exhibited higher photocatalytic activity, especially for the co-doped sample. The MO solution was degraded completely in 3h.

The high porosity, the large pore size and the high pore volume of the mesoporous TiO₂ samples, which were favorable for the adsorption of organic molecules in the mesostructure, led to the improvement of the organic degradation capability. Furthermore, the UV-visible reflection result of the samples indicated that the N, S doping improved the photoadsorption of the light. As a result, the N, S doped mesoporous TiO₂ showed the highest photocatalytic activity among these three samples.

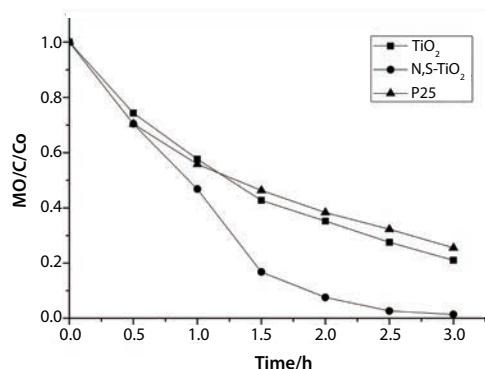


Figure 5. The photocatalytic activity of the pure and N,S co-doped mesoporous TiO₂ samples together with P25.

Summary

The TiO₂ mesoporous materials discussed above, which possess interesting properties and potential applications, constitute an important domain of the nanostructure family. Future developments will rely on facile fabrication processes and novel synthetic methods. Specifically, more work needs to be done to address the combination of sol-gel chemistry with other synthesis techniques to improve both in terms of morphology, purity, composition and yield control and in terms of flexibility for pore size choice.

Acknowledgments

This work is financially supported by Beijing Innovation Talent Project (PHR201006101); Beijing Municipal Commission of Education Key Foundation (KZ2010100050001); National Natural Science Foundation of China (51002004); Beijing New Century Hundred, Thousand and Ten Thousand Talent Project, State key Laboratory of Electronic Thin Films and Integrated Devices (UESTC: KFJJ201001).

References

- Hossain M. F., Biswas S., Takahashia T., Kubota Y., Fujishima A. *J. Vac. Sci. Technol. A* **2008**, *26*, 1007-1011.
- Mukherjee B., Karthik C., Ravishankar N., *J. Phys. Chem. C* **2009**, *113*, 18204-18211.
- Fu T., Liu B. G., Zhou Y. M., Wu X. M., *J. Sol-Gel Sci. Technol.* **2011**, *58*, 307-311.
- Bischoff B. L., and Anderson M. A., *Chem. Mater.* **1995**, *7*, 1772-1778.
- Qiu J., Yu W., Gao X., Li X., *J. Sol-Gel Sci. Technol.* **2007**, *44*, 235-239.
- Liu X., Gu Y., Huang J., *Chem. Eur. J.* **2010**, *16*, 7730-7740.
- Weatherspoon M. R., Cai Y., Crne M., Srinivasarao M., Sandhage K. H., *Angew. Chem. Int. Ed.* **2008**, *47*, 10203-10302.
- Cho C. Y., Moon J. H., *Adv. Mater.* **2011**, *23*, 2971-2975.
- Kaune G., Memesa M., Meier R., Ruderer M. A., Diethert A., Roth S. V., D'Acunzi M., Gutmann J. S., Muller-Buschbaum P., *ACS Appl. Mater. Interfaces* **2009**, *1*, 2862-2869.
- Chen J., Hua Z., Yan Y., Zakhidov A. A., Baughmand R. H., Xu L., *Chem. Commun.* **2010**, *46*, 1872-1874.
- J.H. Pan, X. Zhang, A.J. Du, D.D. Sun and J.O. Leckie, *J. Am. Chem. Soc.* **2008**, *130*, 11256-11257.
- Kim Y. J., Chai S. Y., Lee W. I., *Langmuir* **2007**, *23*, 9567-9571.
- Malfatti L., Bellino M. G., Innocenzi P., Soler-Illia G. J. A. A., *Chem. Mater.* **2009**, *21*, 2763-2769.
- G.J. De, A.A. Soler-Illia, E.L. Crepaldi, D. Grosso and C. Sanchez, *Curr. Opin. Colloid Interface Sci.* **2003**, *8*, 109-126.
- Wu Q. L., Subramanian N., Rankin S. E., *Langmuir* **2011**, *27*, 9557-9566.
- Wang J., Li H., Li H., Zou C., *Solid State Sciences* **2010**, *12*, 490-497.
- Li H., Wang J., Li H., Yin S., Sato T., *Mater. Lett.* **2009**, *63*, 1583-1585.
- C.T. Kresge, M.E. Leonowicz, W.J. Roth, J.C. Vartuli, J.S. Beck, *Nature* **1992**, *359*, 710-712.
- A. Mills, M. Sheik, C. O'Rourke, M. McFarlane, *Appl. Catal. B: Environ.* **2009**, *89*, 189-195.

Titanium Precursors: Alkoxides and Halogenides

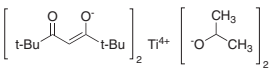
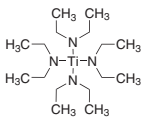
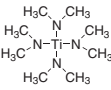
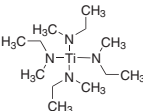
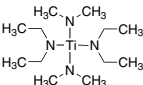
For a complete list of available materials, visit aldrich.com/periodic

Name	Composition	Purity	Description	Prod. No.
Titanium(IV) <i>tert</i> -butoxide	Ti[OC(CH ₃) ₃] ₄	deposition grade	liquid	462551-25ML 462551-50ML
Titanium(IV) butoxide	Ti(OCH ₂ CH ₂ CH ₂ CH ₃) ₄	97%, reagent grade	liquid (or viscous liquid)	244112-5G 244112-100G 244112-500G 244112-2KG
Titanium(IV) butoxide	Ti(OCH ₂ CH ₂ CH ₂ CH ₃) ₄	≥97.0%, gravimetric	liquid	86910-250ML 86910-1L
Titanium(IV) isopropoxide	Ti[OCH(CH ₃) ₂] ₄	99.999% trace metals basis	liquid liquid	377996-5ML 377996-25ML 377996-100ML
Titanium(IV) isopropoxide	Ti[OCH(CH ₃) ₂] ₄	97%	liquid	205273-4X25ML 205273-100ML 205273-500ML 205273-2L
Titanium(IV) propoxide	Ti(OC ₂ H ₅) ₄	98%	liquid	253081-100G 253081-500G
Titanium(IV) 2-ethylhexyloxide	Ti[OCH ₂ CH(C ₂ H ₅)(CH ₂) ₃ CH ₃] ₄	95%	liquid	333484-5ML 333484-250ML
Titanium(IV) ethoxide	Ti(OC ₂ H ₅) ₄	technical grade	liquid	244759-50G 244759-250G
Titanium(IV) methoxide	Ti(OCH ₃) ₄	≥99.99% trace metals basis	powder	463582-25G
Titanium(IV) methoxide	Ti(OCH ₃) ₄	95%	solid	404950-10G 404950-50G
Titanium(IV) oxyacetylacetonate	TiO[CH ₃ COCH=C(O)CH ₃] ₂	90%	powder	330833-10G 330833-50G
Titanium diisopropoxide bis(acetylacetonate)	[(CH ₃) ₂ CHO] ₂ Ti(C ₅ H ₇ O ₂) ₂	75 wt. % in isopropanol	solution	325252-100ML 325252-500ML
Chlorotrisisopropoxytitanium(IV)	[(CH ₃) ₂ CHO] ₃ TiCl	95%	liquid	250627-100G 250627-800G
Chlorotrisisopropoxytitanium(IV) solution	[(CH ₃) ₂ CHO] ₃ TiCl	1.0 M in hexanes	solution	252670-100ML

Name	Composition	Purity	Description	Prod. No.
Titanium(IV) bromide	TiBr ₄	99.99% trace metals basis, anhydrous	powder	451606-1G 451606-5G
Titanium(IV) bromide	TiBr ₄	98%	-	307793-25G 307793-100G
Titanium(II) chloride	TiCl ₂	99.98% trace metals basis, anhydrous	powder	451738-1G 451738-5G
Titanium(III) chloride	TiCl ₃	≥99.995% trace metals basis	crystalline	514381-1G 514381-5G
Titanium(III) chloride	TiCl ₃	ReagentPlus®	powder	220973-5G 220973-25G
Titanium(IV) chloride	TiCl ₄	≥99.995% trace metals basis	liquid	254312-10G 254312-50G
Titanium(III) chloride-aluminum chloride	(TiCl ₃) ₃ · AlCl ₃	-	solid	456411-50G
Titanium(III) fluoride	TiF ₃	-	powder	399817-5G
Titanium(IV) fluoride	TiF ₄	-	powder and chunks	333239-10G 333239-100G
Titanium(IV) iodide	TiI ₄	99.99% trace metals basis, anhydrous	powder	458449-2G

Titanium Volatile Precursors: Thin Film Deposition

For a complete list of available materials, visit aldrich.com/periodic

Name	Structure	Purity	Prod. No.
Titanium(IV) diisopropoxidebis(2,2,6,6-tetramethyl-3,5-heptanedionate)		99.99%	494143-5G
Tetrakis(diethylamido)titanium(IV)		99.999% trace metals basis	469866-5G 469866-25G
Tetrakis(dimethylamido)titanium(IV)		99.999%	469858-5G 469858-25G
Tetrakis(ethylmethylamido)titanium(IV)		≥99.99%	473537-5G
Bis(diethylamido)bis(dimethylamido)titanium(IV)		≥99.99% trace metals basis ≥95%	J100026-10G

Titanium Oxide Nanomaterials

For a complete list of available materials, visit aldrich.com/nanomaterials

Name	Purity	Form	Description	Prod. No.
Titanium(IV) oxide	≥99.5% trace metals basis	nanopowder	particle size ~21 nm, spec. surface area 35-65 m ² /g (BET)	718467-100G
Titanium(III) oxide	99.9% trace metals basis	powder	-100 mesh	481033-10G 481033-50G
Titanium(IV) oxide, anatase	99.7% trace metals basis	nanopowder	particle size <25 nm, spec. surface area 45-55 m ² /g	637254-50G 637254-100G 637254-500G
Titanium(IV) oxide, rutile	99.5% trace metals basis	nanopowder	particle size <100 nm, spec. surface area 130-190 m ² /g	637262-25G 637262-100G 637262-500G
Titanium(IV) oxide, mixture of rutile and anatase	99.5% trace metals basis	nanopowder	particle size <100 nm (BET)	634662-25G 634662-100G
Titanium(IV) oxide, mixture of rutile and anatase	99.9% trace metals basis	nanoparticles paste	particle size <250 nm (DLS), BET surf. area 50 m ² /g	700355-25G
Titanium(IV) oxide, mixture of rutile and anatase	99.9% trace metals basis	dispersion nanoparticles	particle size <150 nm (DLS)	700347-25G 700347-100G
Titanium(IV) oxide, mixture of rutile and anatase	99.9% trace metals basis	dispersion nanoparticles	particle size <100 nm (DLS) BET surf. area 90 m ² /g	700339-100G
Titanium	98.5% trace metals basis	nanoparticles (dispersion)	particle size <100 nm	513415-5G

Precursors for Atomic Layer Deposition

High-Tech Solutions for Your Research Needs

Nano-layers of metals, semiconducting and dielectric materials are crucial components of modern electronic devices, high-efficiency solar panels, memory systems, computer chips and a broad variety of high-performance tools.

The technique of choice for depositing nano-films on various surfaces is Atomic Layer Deposition (ALD), which is a versatile tool for nanostructuring and uses consecutive chemical reactions on a material's surface to create nanostructures with predetermined thickness and chemical composition.¹

Aldrich Materials Science offers high-quality precursors for ALD safely packaged in steel cylinders suitable for use with a variety of deposition systems.

We continue to expand our portfolio of ALD precursors to include new materials. For an updated list of our deposition precursors, visit aldrich.com/aldprecursors

References:

1. Knez, M. *Material Matters* **2008**, 3(2), 28.



Precursors Packaged for Deposition Systems

Precursors are ordered by atomic number of the metallic element.

Description	Acronym	Molecular Formula	Prod. No.
Water packaged for use in deposition systems	-	OH ₂	697125
Trimethylaluminum	TMA	Al(CH ₃) ₃	663301
Tris(dimethylamino)silane	TDMAS	SiH(N(CH ₃) ₂) ₃	759562
Tetraethyl orthosilicate	TEOS	Si(OC ₂ H ₅) ₄	759414
2,4,6,8-Tetramethylcyclotetrasiloxane	TMCTS	(HSiCH ₃ O) ₄	760293
(3-Aminopropyl)triethoxysilane	APTS	Si((CH ₂) ₃ NH ₂)(OC ₂ H ₅) ₃	706493
Silicon tetrachloride	STC	SiCl ₄	688509
Tris(<i>tert</i> -butoxy)silanol	TBS	Si(OH)(OC(CH ₃) ₃) ₃	697281
Tris(<i>tert</i> -pentoxy)silanol	TPS	Si(OH)(OC(CH ₃) ₂ (C ₂ H ₅) ₃) ₃	697303
Tetrakis(diethylamido)titanium(IV)	TDEAT	Ti(NC ₂ H ₅) ₄	725536
Tetrakis(dimethylamido)titanium(IV)	TDMAT	Ti(N(CH ₃) ₂) ₄	669008
Titanium tetrachloride	TTC	TiCl ₄	697079
Titanium(IV) isopropoxide	TTIP	Ti(OCH(CH ₃) ₂) ₄	687502
Vanadium(V) oxytriisopropoxide	VTIP	V(O)(OCH(CH ₃) ₂) ₃	736007
Diethylzinc	DEZ/DEZn	Zn(C ₂ H ₅) ₂	668729
Triethylgallium	TEG/TEGa	Ga(C ₂ H ₅) ₃	730726
Trimethylgallium	TMG/TMGa	Ga(CH ₃) ₃	730734
Tris[<i>N,N</i> -bis(trimethylsilyl)amide] yttrium	YTDMSA	Y(N(CH ₃) ₃ Si) ₃	702021
Zirconium(IV) <i>tert</i> -butoxide	ZTB	Zr(OC(CH ₃) ₃) ₄	759554

Description	Acronym	Molecular Formula	Prod. No.
Bis(methyl-η ⁵ -cyclo-pentadienyl) methoxymethylzirconium	ZRCMMM/ ZRD-CO4	Zr(CH ₃ C ₅ H ₄) ₂ CH ₃ OCH ₃	725471
Tetrakis(dimethylamido)zirconium(IV)	TDMAZ	Zr(N(CH ₃) ₂) ₄	669016
Tetrakis(ethylmethylamido) zirconium(IV)	TEMAZ	Zr(N(CH ₃)(C ₂ H ₅) ₂) ₄	725528
Niobium(V) ethoxide	NbOEt	Nb(OCH ₂ CH ₃) ₅	760412
Bis(ethylcyclopentadienyl) ruthenium(II)	Ru(EtCp)2	Ru(C ₅ H ₄ (C ₂ H ₅) ₂) ₂	679798
Bis(methyl-η ⁵ -cyclopentadienyl) dimethylhafnium	HFCMME/ HfD-CO2	Hf(C ₅ H ₄ (CH ₃) ₂) ₂ (CH ₃) ₂	725501
Bis(methyl-η ⁵ -cyclopentadienyl) methoxymethylhafnium	HfD-CO4	Hf(CH ₃ (OCH ₃)) ₂ [(C ₅ H ₅ (CH ₃) ₂) ₂	725498
Tetrakis(dimethylamido)hafnium(IV)	TDMAH	Hf(N(CH ₃) ₂) ₄	666610
Tetrakis(ethylmethylamido) hafnium(IV)	TEMAH	Hf(N(CH ₃)(C ₂ H ₅) ₂) ₄	725544
Tris(diethylamido)(<i>tert</i> -butylamido) tantalum(V)	TBTDDET	Ta(NC(CH ₃) ₂) ₃ [N(C ₂ H ₅) ₂] ₃	668990
Bis(<i>tert</i> -butylamido) bis(dimethylamino)tungsten(VI)	BTBMW	W(N(CH ₃) ₂) ₂ (NC(CH ₃) ₂) ₂	668885
Trimethyl(methylcyclo-pentadienyl) platinum(IV)	MeCpPtMe3	Pt(C ₅ H ₄ CH ₃)(CH ₃) ₃	697540

For additional vapor deposition precursors prepacked in cylinders, please contact us by email at matsci@sial.com.

Synthesis of Melting Gels Using Mono-Substituted and Di-Substituted Alkoxysiloxanes



Lisa C. Klein^{1*} and Andrei Jitianu²

¹Rutgers University
Department of Materials Science and Engineering
607 Taylor Road, Piscataway, NJ 08854.

²Lehman College, City University of New York
Department of Chemistry, Davis Hall
250 Bedford Park Boulevard West, Bronx, NY 10468, USA.

*Email: licklein@rci.rutgers.edu

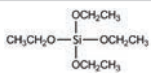
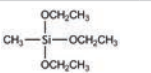
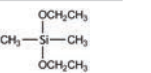
Introduction to Organic-Inorganic Hybrid Gels

Hybrid organic-inorganic sol-gel materials containing silica were first called "ORMOSILs" in 1984.¹ Since then, the number of hybrid organic-inorganic combinations has increased rapidly.² Hybrid materials have remarkable features resulting from the synergistic combination of both inorganic and organic components that make them suitable for a wide range of applications such as electrochemical devices, biomedical applications including drug delivery, and electronic and optoelectronic applications including light-emitting diodes, photodiodes, solar cells, gas sensors and field effect transistors.

Generally, organic-inorganic materials are classified in two broad categories: Class I materials where the organic and inorganic components are embedded one within the other and display weak bonds, and Class II materials where there are strong covalent bonds between the inorganic and organic components.³

For more than 25 years hybrid gels have been grown by sol-gel process.⁴ Since sol-gel processing is a low temperature method, it is only natural that sol-gel processing has been extended to hybrid materials with retained organic content. Ordinarily, the outcome of the sol-gel process with the precursor tetraethylorthosilicate (TEOS) (Aldrich Prod. No. 333859) is a 3-dimensional network. TEOS, with 4 identical groups attached to Si, undergoes hydrolysis and polycondensation reactions. The 4 identical groups can be changed to, for example, 3 identical groups and one group with a direct Si-C bond. While the remaining 3 ethoxy groups are reactive to hydrolysis, the substituted group, for example, methyl, is not.

Below is a schematic (Scheme 1) of the number of reactive groups, as the ethoxy group on TEOS is substituted successively by methyl:

Name	Tetraethoxysiloxane	Methyltriethoxy-siloxane	Dimethyldiethoxy-siloxane
Abbreviation	TEOS	MTES	DMEDES
Aldrich Product Number	333859	339644	175595
Structure			
Number of Reactive Groups	4	3	2
Number of Nonreactive Substitutions	0	1	2
Relative Reactivity ⁵	Intermediate	Most	Least

Substituting groups besides methyl that have been studied include ethyl, phenyl, and vinyl. The size and polarity of the groups influences the properties. A common precursor among Class II hybrids for thin films is methyltriethoxysiloxane (MTES) (Aldrich Prod. No. 339644), $\text{CH}_3\text{Si}(\text{OC}_2\text{H}_5)_3$, together with tetraethoxysiloxane (TEOS), $\text{Si}(\text{OC}_2\text{H}_5)_4$.⁶ The retention of the methyl groups in the films reduces tension and lessens cracking. More complicated ORMOSILs are obtained by co-condensation of TEOS with MTES and vinyltriethoxysiloxane (Aldrich Prod. No. 679275) and 3-glycidoxy-propyltrimethoxysiloxane (Aldrich Prod. No. 440167).^{7,8}

In addition to the beneficial effects of retained organic content on mechanical properties, there are interesting effects on hybrid gel surface chemistry, which are reflected in hydrophobicity or hydrophilicity. For example, a water-repelling surface, which has a contact angle greater than 90°, can be tailored through the choice of organic groups on the surface. For silica-based hybrids, the affinity for water can be decreased by reducing the number of the vicinal -OH groups.⁹ Reducing the -OH groups can be achieved by replacing them with hydrophobic groups such as methyl.¹⁰ In this way, organic-inorganic coatings have been developed for anti-graffiti, anti-adhesive and anti-static coatings, among others.¹¹ Since the refractive index and the thickness of hybrid coatings can be adjusted, waveguides based on phenyltriethoxysiloxane (PhTES) (Aldrich Prod. No. 679291), MTES and TEOS have been patterned by microfluidic lithography.¹²

Discovery of Melting Gel Behavior

Recently, it has been found that Class II hybrids, which are mixtures of di-substituted and mono-substituted alkoxysiloxanes, can produce so-called melting gels with a range of softening behaviors and a range of temperatures where the gel flows.¹³ These hybrids originally were investigated to replace low melting temperature sealing glasses that melt around 600 °C. This temperature is too high for most electronic packaging, especially newer devices with organic light emitting diodes (OLED).

Melting gels are rigid at room temperature, soften at around 110 °C and consolidate at temperatures above 130 °C. The process of (a) softening, (b) becoming rigid and (c) re-softening can be repeated many times, until heated above 130 °C after which the gel no longer softens.¹³

While the softening behavior has been called melting, it is not melting in a thermodynamic sense.¹⁴ At the same time, it is not thixotropic behavior either, as the material cannot be caused to flow by shearing. Instead, the ability to soften and flow is a behavior seen in some but not all combinations of mono-substituted and di-substituted alkoxysiloxanes, indicating incomplete crosslinking. In fact, melting gels show glass transition behavior at temperatures below 0 °C.

One of the first mentions of "melting gels" involved poly(benzyl-silsesquioxane) (POSS) particles, which were deposited onto an indium-tin oxide (ITO) (Aldrich Prod. Nos. 749745, 749796) coated substrate by electrophoretic deposition. After heat treatment at very low temperatures, continuous thick transparent films were obtained.¹⁴ Using a different approach with PhTES and DPhDES (diphenyldiethoxysiloxane) (Aldrich Prod. No. D83532), poly-silsesquioxanes were obtained that showed a low softening point. PhTES-DPhDES hybrids could be formed with or without ethanol as monodisperse particles, and the glass transition temperature of these hybrids varied with ratio of PhTES and DPhDES.¹⁵⁻¹⁷



In comparing the methyl substituted melting gels with ethoxy (MTES/DMEDES), with methoxy (MTMS/DMDMS) and their phenyl-substituted melting gel analogs (PhTES/DPhDES and PhTMS/DPhDMS), it was found that melting gels occurred for different mixtures, depending on the system. The methyl-substituted alkoxysiloxanes show melting gel behavior over a wide range of compositions, while the phenyl-substituted compositions are a majority of the mono-substituted alkoxysiloxane, going so far as to have melting gels with only PhTES or PhTMS.¹³

Now that melting gel behavior has been studied in a more systematic way, a family of organically modified silica gels made up of mixtures of mono-substituted alkoxysiloxanes and di-substituted alkoxysiloxanes has been characterized and their properties such as contact angle with water¹⁰, density¹⁸, and hermeticity have been investigated.¹⁸

Precursors for Melting Gels

While the catalog of alkoxysiloxanes is almost limitless, two typical precursors for melting gels are listed in **Table 1**, along with TEOS for comparison. Note that all of the precursors are liquids at room temperature, and are described as reacting slowly with water at room temperature.

Table 1: Precursors Investigated for Melting Gels, with TEOS for comparison.

Chemical Name	Formula	Molecular Weight (g/mol)	Melting Point (°C)	Boiling Point (°C)	Specific Gravity	% Oxide
DMEDES	C ₆ H ₁₆ O ₂ Si	148.28	-97	114	0.865	40.5
MTES	C ₇ H ₁₈ O ₃ Si	178.3	-50	142	0.895	33.7
TEOS	C ₈ H ₂₀ O ₄ Si	208.33	-77	169	0.9335	28.8

Synthesis of Melting Gels Using Mono-Substituted and Di-Substituted Alkoxysiloxanes

In a typical synthesis, the MTES and DMEDES are used without further purification. Hydrochloric acid and ammonia are used as catalysts. Anhydrous ethanol is the solvent. A total of 5 gels were prepared with the indicated mol% of MTES and DMEDES listed in **Table 2**. The synthesis flowchart is shown in **Figure 1**, and described step-by-step.

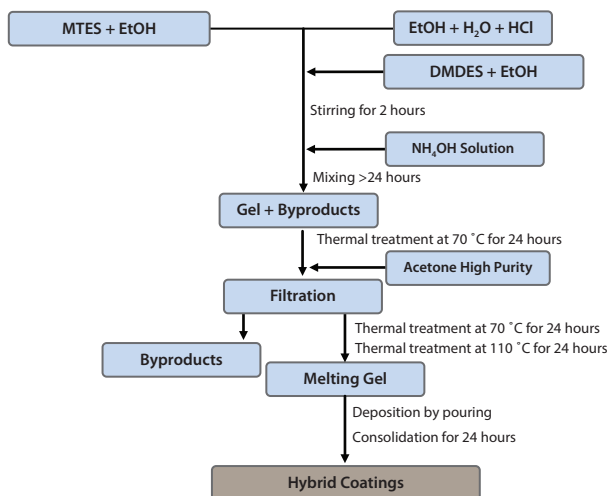


Figure 1. Flow chart of the synthesis of melting gels using MTES and DMEDES.

The synthesis has three steps. First the water is mixed with hydrochloric acid and half of the ethanol. The MTES is mixed with the other half of the ethanol separately. Then, the ethanol mixed with MTES is added dropwise to the water solution under continuous stirring. The beaker is covered tightly, and the mixture is stirred at room temperature for 3 hours.

In the second step, DMEDES is diluted with ethanol. The DMEDES in ethanol mixture is added dropwise to the mixture from the first step. This solution is kept in a closed beaker at room temperature for another two hours of stirring.

In the third step, ammonia is added to the reaction mixture and the solution is stirred for another hour in a closed beaker. Then the clear solution is stirred for 48 hours at room temperature in an open beaker until gelation occurs. The gels are heat treated at 70 °C overnight to remove excess ethanol. During this process, a white powder of ammonium chloride forms on the gels. To remove the ammonium chloride, 10 mL of acetone are added to the samples, followed by removal by vacuum filtration. Again, the gels are heat treated at 70 °C for 24 hours, followed by a last heat treatment at 110 °C for removal of un-reacted water.

After this heat treatment, the gels are rigid at room temperature. However, when heated above ~110 °C, the gels soften and become fluid, in some cases as fluid as water. To locate the consolidation temperature, samples were subjected to heating and cooling cycles until the minimum temperature is found after which the gels could not be softened. Once the gel had been heated to the consolidation temperature, the behavior was no longer reversible. The consolidation temperatures (T_{CON}) are listed in **Table 2**.

The thermal behavior of the hybrid gels before consolidation was studied using differential thermal analysis (Perkin-Elmer DTA-7), thermogravimetric analysis (Perkin-Elmer TGA-7) and differential scanning calorimetry (DSC TA-Q-2000).¹⁹ The glass transition temperatures were determined and are listed in **Table 2**.

Table 2: Relationship between composition and properties of melting gels.

Monosubstituted (mol %) MTES	Disubstituted (mol %) DMEDES	T_g (°C)	T_{CON} (°C)	Total Weight Loss (%)	Calculated Weight Loss (%)
50	50	-56.7	160	45	62.9
60	40	-37.7	155	37	63.6
65	35	-18.8	150	35	63.9
70	30	-6.4	145	34	64.3
75	25	-0.3	135	30	64.6

Results and Discussion

The weight loss for all gels occurred in two temperature ranges. At lower temperatures between about 150 °C and 300 °C, the weight loss is attributed to the removal of the ethoxy and hydroxyl groups. The second weight loss occurs between about 350 °C and 500 °C due to the combustion of the methyl groups. For all samples, the differential thermal analysis shows an exothermic peak accompanying the high temperature weight loss, confirming the combustion of the methyl groups.

The measured weight loss increases with the concentration of the di-substituted alkoxyloxane. Considering that the calculated weight loss, based on formula weight and full oxidation to silica, varies little among the compositions, it is interesting to see the measured trend. The consolidation temperature trends in the same direction as the weight loss, as shown in **Table 2**.

The consolidation temperatures listed in **Table 2** decreases with a decrease in the amount of di-substituted alkoxyloxane. This decrease in the consolidation temperature is consistent with the fact that di-substituted alkoxyloxanes have only two reactive sites available to create new bonds with the rest of the silica network, while mono-substituted alkoxyloxanes have three. Without the mono-substituted alkoxyloxane, the di-substituted alkoxyloxanes remain liquid after hydrolysis and polycondensation reactions because only linear chains are formed. When mono-substituted alkoxyloxanes are mixed with the di-substituted alkoxyloxanes, the di-substituted alkoxyloxanes act as bridges between the molecular species formed when the mono-substituted alkoxyloxanes hydrolyze.

The glass transition temperatures listed in **Table 2** show the opposite trend to the consolidation temperature. The T_g values increase with decreasing amount of di-substituted alkoxyloxanes. The glass transition is generally thought of as the interval of transition between liquid states and glassy, amorphous states. Put another way, the glass transition reflects a number of macroscopic properties, such as viscosity, dielectric constant, and mechanical properties. Using the approach developed for traditional organic polymers and applied to inorganic silica-based polymers, the glass transition temperature is considered a measure of the degree of cross-linking in the silica network. In other words, the T_g increases with an increase in the number of oxygen bridges between silicon atoms.

After gelation and heat treatment to remove solvents and water, the gels are rigid. An example of a melting gel is shown in **Figure 2**. A beaker with a rigid layer of gel on the bottom is turned on its side. This is the appearance of the melting gel after gelation, but before consolidation. Then, the beaker is placed on a hot plate and warmed to a modest 110 °C. The tilted beaker with the softened gel is shown in **Figure 3**. The gel has softened and is beginning to flow because the beaker is tilted. Most of the combinations soften to a viscosity between water and syrup, making pouring easy. When the fluid gel was poured onto a variety of substrates, including glass, mica, silicon, copper and aluminum, the gel adhered well to all surfaces. Thick films were about 1 mm thick and relatively smooth. In addition, the films are transparent and show no tackiness. The thick films have been heated to their consolidation temperatures, after which a variety of physical properties, such as contact angle, hardness and permeability, have been measured and reported.²⁰



Figure 2. Beaker containing melting gel before heating on its side.



Figure 3. Beaker tilted after warming to soften the gel so that it can be poured.

Applications of Melting Gels for “low- κ ” Dielectrics

The property requirements for low- κ materials in integrated circuits for simple metal-oxide semiconductor field effect transistors (MOSFET) include structural uniformity, low dielectric constant ($\kappa \sim 2$), low dielectric loss, high hardness, high adhesion strength, thermal stability, and low moisture absorption.²¹ Many of these characteristics can be satisfied by melting gels. The network structure in organically modified silica melting gels helps them achieve the structural uniformity and hardness. Also, the fact that SiO_2 has a low κ by itself means that the dielectric constant of the melting gel can be close to 2 with appropriate amount of organic component and possibly some closed porosity. In addition, the silica content of the hybrid gives thermal stability to the low κ material. Melting gels have low viscosity at their softening temperature, so they can be applied by spin coating. The coatings show good adhesion to silicon substrates, and melting gels show very low vapor transport values.²² For all of these reasons, melting gels are interesting materials to consider for multilevel interconnect structures.

One composition that looks promising for low- κ dielectrics is the 65% MTES - 35% DMDES gel, which has a high value of the contact angle ($\theta = 100^\circ$), negligible BET surface area (0.0138 m^2/g) and a low density (1.252 g/cm^3). The dielectric constant is about 4.2 at 1KHz.²³

Conclusions

A combination of mono-substituted and di-substituted alkoxyloxanes, reacted using a three-step synthesis, results in a so-called melting gel. The alkoxyloxanes undergo hydrolysis and condensation polymerization similar to a conventional sol-gel process. Hydrochloric acid in the first step promotes the formation of linear polymer chains. Ammonia in the third step serves to neutralize the hydrochloric acid and to promote cross-linking between the polymer chains, which leads to gelation. Incomplete cross-linking is reflected in the glass transition temperature T_g of the gels before consolidation. The melting gels can be softened repeatedly. However, once the gels have been heated to their consolidation temperature, they no longer soften. After consolidation, the gels are hard and impermeable.

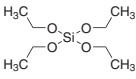
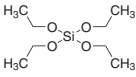
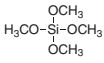
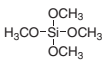
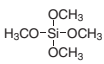
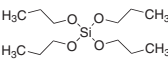
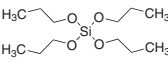
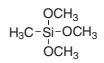
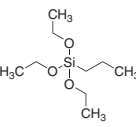
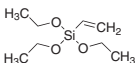
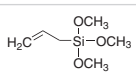
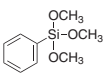


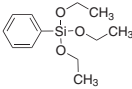
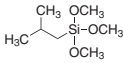
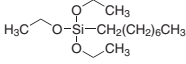
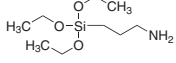
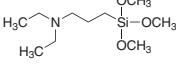
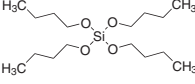
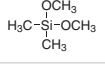
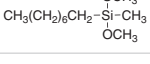
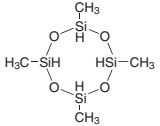
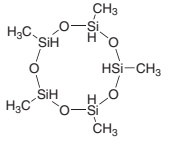
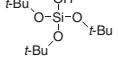
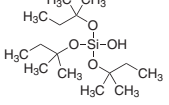
References

- Schmidt, H. *Mat. Res. Soc. Symp. Proc.* **1984**, *32*, 327-335.
- Avnir, D., Klein, L. C., Levy, D., Schubert, U., Wojcik, A. B., in *The Chemistry of Organosilicon Compounds Vol. 2*, eds. Z. Rappoport and Y. Apeloig, Wiley, London, **1998**, Chapter 40, pp. 2317-2362.
- Sanchez, C., Ribot, F. *New J. Chem.* **1994**, *10*, 1007-1040.
- Klein, L. C. *Ann. Rev. Mater. Sci.* **1985**, *15*, 227-48.
- Liu, R., Xu, Y., Wu, D., Sun, Y., Gao, H., Yuan, H., Deng, F., *J. Non-Cryst. Solids* **2004**, *343*, 61-70.
- Orel, B., Jese, R., Vilcnik, A., Lavrencic-Stangar, U. *J. Sol-Gel Sci. & Tech.* **2005**, *34*, 251-265.
- Jackson, A., Jitianu, A., Klein, L. C. *Material Matters* (Sigma-Aldrich) **2006**, *1* (3), 11-12.
- Chan, Z., Ai'mei, L., Xiao, Z., Miao, F., Juan, H., Hongbing, Z. *Optic. Mater.* **2007**, *29*, 1543-1547.
- Castricum, H. L., Sah, A., Mittelmeijer-Hazeleger, M. C., Huiskes, C., ten Elshof, J. E. *J. Mat. Chem.* **2007**, *17*, 1509-1517.
- Jitianu, A., Amatucci, G., Klein, L. C. *J. Materials Research* **2008**, *23*, 2084-2090.
- Hass, K. H., Amberg-Schwab, S., Rose, K. *Thin Solid Films* **1999**, *351*, 198-203.
- Jeong, S., Ahn, S.-J., Moon, J. *J. Am. Ceram. Soc.* **2005**, *88*, 1003-1036.
- Klein, L. C., Jitianu, A. *J. Sol-Gel Science & Tech.* **2010**, *55*, 86-93.
- Matsuda, A., Sasaki, T., Hasegawa, K., Tatsumisago, M., Minami, T. *J. Am. Ceram. Soc.* **2001**, *84*, 775-780.
- Kakiuchida, H., Takahashi, M., Tokuda, Y., Masai, H., Kuniyoshi, M., Yoko, T. *J. Phys. Chem. B* **2007**, *111*, 982-988.
- Takahashi, K., Tadanaga, K., Hayashi, A., Matsuda, A., Tatsumisago, M. *J. Cer. Soc. Jpn.* **2007**, *115*, 131-135.
- Jitianu, A., Amatucci, G., Klein, L. C. *J. Am. Ceram. Soc.* **2008**, *92*, 36-40.
- A. Jitianu, A., Doyle, J., Amatucci, G., Klein, L. C., Proceedings MS&T 2008 *Enabling Surface Coating Systems: Multifunctional Coatings* (CD-ROM), Pittsburgh, PA, 2008, pp. 2171-2182.
- Jitianu, A., Lammers, K., Arbuckle-Keil, G. A., Klein, L. C. *Journal of Therm. Anal. Calorim.* **2012**, *107*, 1039-1045.
- Jitianu, A., Doyle, J., Amatucci, G., Klein, L. C. *J. Sol-Gel Science & Tech.* **2010**, *53*, 272-279.
- Hatton, B. D., Landskron, K., Hunks, W. J., Bennett, M. R., Shukaris, D., Petrovic, D. D., Ozin, G. A. *MaterialsToday* **2006**, *9*, 22-31.
- Jitanu, A., Gambino L., Klein, L. C., in *Sol-Gel Processing for Conventional and Alternative Energy*, ed. M. Aparicio, A. Jitianu and L. C. Klein, Springer, New York, 2012, pp. 375-392 DOI:10.07/978-1-4614-1957-0.
- Gambino, L., Jitianu, A., Klein, L. C. *J. Non-Cryst. Solids* **2012**, DOI:10.1016/j.jnoncrysol.2012.01.002.

Silicon Precursors for Hybrid and Melting Gels: Silicates and Siloxanes

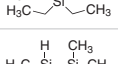
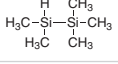
For a complete list of available materials, visit aldrich.com/mnel

Name	Structure	Purity	Prod. No.
Tetraethyl orthosilicate		99.999% trace metals basis	333859-25ML 333859-100ML
Tetraethyl orthosilicate		98%	131903-25ML 131903-250ML 131903-500ML 131903-1L 131903-2.5L 131903-4L
Tetramethyl orthosilicate		≥98% ≥99.9% trace metals basis	679259-50G
Tetramethyl orthosilicate		≥99%	341436-25G 341436-100G
Tetramethyl orthosilicate		98%	218472-100G 218472-500G
Tetrapropyl orthosilicate		≥98%	679240-50G
Tetrapropyl orthosilicate		95%	235741-25G 235741-100G
Trimethoxymethylsilane		≥98%	679232-50G
n-Propyltriethoxysilane		≥98%	679321-50G
Triethoxyvinylsilane		≥98%	679275-50G
Allyltrimethoxysilane		≥98%	679267-50G
Trimethoxyphenylsilane		≥98%	679313-50G

Name	Structure	Purity	Prod. No.
Triethoxyphenylsilane		≥98%	679291-50G
Isobutyl(trimethoxy)silane		≥98%	679364-50G
Triethoxy(octyl)silane		98% 99.99% trace metals basis	679305-50G
(3-Aminopropyl)triethoxysilane		≥98.0%	741442-100ML 741442-500ML
[3-(Diethylamino)propyl]trimethoxysilane		≥98%	679356-50G
Tetraethyl orthosilicate		97%	T5702-100G
Tetramethylammonium silicate solution	$(\text{CH}_3)_4\text{N}(\text{OH}) \cdot 2\text{SiO}_2$	≥99.99% trace metals basis	438669-100ML 438669-500ML
Dimethoxydimethylsilane		≥99.5% 99.999% metals basis	556688-25ML
Dimethoxy(methyl)octylsilane		≥95.0%, GC	68215-25ML
2,4,6,8-Tetramethylcyclotetrasiloxane		≥99.999% trace metals basis ≥99.5%	512990-25ML 512990-100ML
2,4,6,8,10-Pentamethylcyclopentasiloxane		96%	517801-25ML
Tris(<i>tert</i> -butoxy)silanol		99.999%	553468-5G 553468-25G
Tris(<i>tert</i> -pentoxy)silanol		≥99.99%	553441-5G 553441-25G

Silicon Precursors for Hybrid and Melting Gels: Silanes

For a complete list of available materials, visit aldrich.com/mnel

Name	Structure	Purity	Prod. No.
1,1,2,2-Tetramethyldisilane		98%	445126-1G
Tetramethylsilane		≥99.99% trace metals basis	523771-100ML
Tetraethylsilane		99%	510874-5ML 510874-25ML
Pentamethyldisilane		97%	557641-5ML



Name	Structure	Purity	Prod. No.
Hexamethyldisilane	$\begin{array}{c} \text{H}_3\text{C} \quad \text{CH}_3 \\ \quad \\ \text{H}_3\text{C}-\text{Si}-\text{Si}-\text{CH}_3 \\ \quad \\ \text{H}_3\text{C} \quad \text{CH}_3 \end{array}$	98%	217069-5G 217069-10G 217069-50G
1,2-Dimethyl-1,1,2,2-tetraphenyldisilane		97%	477753-5G
Methylsilane	$\text{H}_3\text{Si}-\text{CH}_3$	$\geq 99.9\%$	462993-10G 462993-20G

Silicon Precursors for Hybrid and Melting Gels: Chlorosilanes and Halogenides

For a complete list of available materials, visit aldrich.com/mnel

Name	Structure	Purity	Prod. No.
Methyltrichlorosilane	$\begin{array}{c} \text{Cl} \\ \\ \text{H}_3\text{C}-\text{Si}-\text{Cl} \\ \\ \text{Cl} \end{array}$	$\geq 98\%$, GC $\geq 99.99\%$ (as metals)	679208-50G
Ethyltrichlorosilane	$\begin{array}{c} \text{Cl} \\ \\ \text{H}_3\text{C}-\text{CH}_2-\text{Si}-\text{Cl} \\ \\ \text{Cl} \end{array}$	$\geq 98\%$, GC $\geq 99.99\%$ (as metals)	679216-50G
Butyltrichlorosilane	$\begin{array}{c} \text{Cl} \\ \\ \text{H}_3\text{C}-\text{CH}_2-\text{CH}_2-\text{Si}-\text{Cl} \\ \\ \text{Cl} \end{array}$	$\geq 98\%$	679224-50G
Pentyltrichlorosilane	$\begin{array}{c} \text{Cl} \\ \\ \text{CH}_3(\text{CH}_2)_3\text{CH}_2-\text{Si}-\text{Cl} \\ \\ \text{Cl} \end{array}$	$\geq 98\%$	679194-50G
Chloropentamethyldisilane	$\begin{array}{c} \text{Cl} \quad \text{CH}_3 \\ \quad \\ \text{H}_3\text{C}-\text{Si}-\text{Si}-\text{CH}_3 \\ \quad \\ \text{H}_3\text{C} \quad \text{CH}_3 \end{array}$	97%	490407-5G
1,2-Dichlorotetramethyldisilane	$\begin{array}{c} \text{Cl} \quad \text{Cl} \\ \quad \\ \text{H}_3\text{C}-\text{Si}-\text{Si}-\text{CH}_3 \\ \quad \\ \text{H}_3\text{C} \quad \text{CH}_3 \end{array}$	95%	415456-5ML
Silicon tetrabromide	SiBr_4	99.995% trace metals basis	494100-5ML 494100-25ML
Silicon tetrabromide	SiBr_4	99%	333468-10G 333468-50G
Silicon tetrachloride	SiCl_4	99.998% trace metals basis	289388-100ML 289388-800ML
Silicon tetrachloride	SiCl_4	99%	215120-100G 215120-1KG

Silicon Precursors for Hybrid and Melting Gels: Silylamines and Silazanes

For a complete list of available materials, visit aldrich.com/mnel

Name	Structure	Purity	Prod. No.
<i>N</i> -sec-Butyl(trimethylsilyl)amine	$\begin{array}{c} \text{H} \quad \text{CH}_3 \\ \quad \\ \text{H}_3\text{C}-\text{CH}_2-\text{N}-\text{Si}-\text{CH}_3 \\ \quad \\ \text{CH}_3 \quad \text{CH}_3 \end{array}$	98%	654671-5G
1,3-Diethyl-1,1,3,3-tetramethyldisilazane	$\begin{array}{c} \text{H}_3\text{C} \quad \text{CH}_3 \\ \quad \\ \text{H}_3\text{C}-\text{Si}-\text{N}-\text{Si}-\text{CH}_3 \\ \quad \\ \text{CH}_3 \quad \text{CH}_3 \end{array}$	$> 98.0\%$	646261-1G 646261-5G
<i>N,N,N'</i> -Tri- <i>tert</i> -butylsilylanetriamine	$\begin{array}{c} \text{H} \quad \text{t-Bu} \\ \quad \\ \text{t-Bu}-\text{N}-\text{Si}-\text{N}-\text{t-Bu} \\ \quad \\ \text{H} \quad \text{H} \end{array}$	99.99% trace metals basis	475386-5ML 475386-10ML
Hexamethyldisilazane	$\begin{array}{c} \text{H}_3\text{C} \quad \text{CH}_3 \\ \quad \\ \text{H}_3\text{C}-\text{Si}-\text{N}-\text{Si}-\text{CH}_3 \\ \quad \\ \text{CH}_3 \quad \text{CH}_3 \end{array}$	99.9%	379212-25ML 379212-100ML
Hexamethyldisilazane	$\begin{array}{c} \text{H}_3\text{C} \quad \text{CH}_3 \\ \quad \\ \text{H}_3\text{C}-\text{Si}-\text{N}-\text{Si}-\text{CH}_3 \\ \quad \\ \text{CH}_3 \quad \text{CH}_3 \end{array}$	$\geq 99\%$	440191-100ML 440191-1L

Wafers and Substrates

For a complete list of available materials, visit aldrich.com/substrates

Name	Composition	Description	Dimensions	Prod. No.
Magnesium oxide	MgO	single side polished, (single crystal substrate)	L x W x thickness 10 x 10 x 0.5 mm	634646-1EA
Magnesium oxide	MgO		L x W x thickness 10 x 10 x 0.5 mm	634697-1EA
Magnesium oxide	MgO		L x W x thickness 10 x 10 x 0.5 mm	634700-1EA
Magnesium aluminate	MgO·Al ₂ O ₃	single crystal substrate single side polished	10 x 10 x 0.5 mm	635073-1EA
Magnesium aluminate	MgO·Al ₂ O ₃	single crystal substrate	10 x 10 x 0.5 mm	634840-1EA
Magnesium aluminate	MgO·Al ₂ O ₃	single crystal substrate single side polished	10 x 10 x 0.5 mm	634832-1EA
Aluminum oxide	Al ₂ O ₃	Crystallographic D spacing ((1120) – a plane: 2.379 Angstrom) Crystallographic D spacing ((1011) – s plane: 1.961 Angstrom) Crystallographic D spacing ((1102) – r plane: 1.740 Angstrom) Crystallographic D spacing ((1040) – m plane: 1.375 Angstrom) Crystallographic D spacing ((0001) – c plane: 2.165 Angstrom) Crystallographic D spacing ((1123) – n plane: 1.147 Angstrom) single crystal substrate single side polished	10 x 10 x 0.5 mm	634875-1EA 634875-5EA
Silicon dioxide	SiO ₂	single crystal substrate	L x W x thickness 10 x 10 x 0.5 mm	634867-5EA
Silicon	Si	crystalline (cubic (a = 5.4037)) wafer	diam. x thickness 2 in. x 0.5 mm	647705-1EA
Silicon	Si	crystalline (cubic (a = 5.4037)) wafer (single side polished)	diam. x thickness 2 in. x 0.5 mm	647675-1EA 647675-5EA
Silicon	Si		diam. x thickness 2 in. x 0.5 mm	647780-1EA 647780-5EA
Silicon	Si		diam. x thickness 2 in. x 0.5 mm	647799-1EA 647799-5EA
Silicon	Si		diam. x thickness 2 in. x 0.5 mm	646687-1EA 646687-5EA
Silicon	Si		diam. x thickness 2 in. x 0.5 mm	647101-1EA 647101-5EA
Silicon	Si		diam. x thickness 3 in. x 0.5 mm	647535-1EA 647535-5EA
Silicon	Si		diam. x thickness 3 in. x 0.5 mm	647543-1EA 647543-5EA
Silicon	Si		diam. x thickness 3 in. x 0.5 mm	647764-1EA 647764-5EA
Silicon	Si		diam. x thickness 3 in. x 0.5 mm	647772-5EA
Silicon	Si		diam. x thickness 3 in. x 0.5 mm	647802-1EA
Silicon	Si		diam. x thickness 3 in. x 0.5 mm	647810-5EA 647810-1EA
Titanium(IV) oxide, rutile	TiO ₂	single side polished	L x W x thickness 10 x 10 x 0.5 mm	635049-1EA
Titanium(IV) oxide, rutile	TiO ₂	single crystal substrate	L x W x thickness 10 x 10 x 0.5 mm	635057-1EA
Titanium(IV) oxide, rutile	TiO ₂		L x W x thickness 10 x 10 x 0.5 mm	635065-1EA
Gold coated microscope slide	Au	-	L x W x thickness 3 in. x 1 in. x 0.7 mm layer thickness 100 Å	643203-5EA
Gold coated microscope slide	Au		L x W x thickness 3 in. x 1 in. x 0.7 mm layer thickness 1000 Å	643246-5EA
Gold coated silicon wafer	Au		diam. x thickness 4 in. x 500 µm layer thickness 1000 Å	643262-1EA
Gold coated mica	Au		L x W x thickness 1 in. x 1.5 in. x 150 µm layer thickness 2000 Å	643270-1EA
Gold coated mica	Au		L x W x thickness 3 in. x 1 in. x 150 µm layer thickness 2000 Å	643297-1EA
Gold coated glass cover slip	Au		diam. x thickness 15 mm x 130-170 µm layer thickness 100 Å	643289-24EA

Nanostructured Materials Through Ultrasonic Spray Pyrolysis



Jin Ho Bang,^{1,2} Yuri T. Didenko,³ Richard J. Helmich,^{1,4} and Kenneth S. Suslick^{1*}
¹School of Chemical Sciences, University of Illinois at Urbana-Champaign, 600 S. Mathews Av., Urbana, IL 61801 USA

²Current address: Department of Chemistry and Applied Chemistry, Hanyang University, 55 Hanyangdaehak-ro, Sangnok-gu, Ansan, Kyeonggi-do 426-791, Republic of Korea

³UT Dots, Inc., 2716 W. Clark Rd, Suite E, Champaign, IL 61822 USA

⁴Current Address: Dept. of Labor, Mine Safety and Health Administration, 6th Ave. and Kipling Pkwy, Bldg 25, Denver, CO 80225

*Email: ksuslick@illinois.edu

Introduction

Advances in materials have often been led by the development of new synthetic methods that provide control over size, morphology and structure. The preparation of materials in a scalable and continuous manner is critical when development moves beyond lab-scale quantities. The ease and scalability for preparing materials has been a driving force for the development of new methodologies for several decades.¹ In this respect, the development of aerosol syntheses has been particularly successful.² Spray pyrolysis has been widely used in industry for preparing fine powders, in addition to thin film deposition. This technique has been generally accepted because the apparatus is simple, continuous, and easily scaled up to mass production. In general, spray pyrolysis involves the thermal reactions of aerosols (i.e., solid or liquid droplets suspended in a gas) generated by a nebulizer (e.g. pneumatic, ultrasonic, or electrostatic) carried in a gas flow through a furnace.

Among the various nebulization techniques available (Table 1), the use of ultrasonic nebulizers has been favored because of their outstanding energy efficiency in aerosol generation, affordability, and the inherent low velocity of the initially formed aerosol. Ultrasonic spray pyrolysis (USP) has been shown to be particularly effective for the preparation of a wide array of materials, and it has the advantage of being highly scalable and continuous.^{3,4} Like sol gel process, USP technique is also a solution based method wherein high frequency ultrasound is passed through a liquid precursor solution, impinging on a liquid-gas interface, which forms an aerosol of micron-sized liquid droplets. The ultrasonically generated droplets of reaction precursors thus become individual chemical microreactors as they are carried by gas flow into a heated furnace where reactions occur. Evaporation of volatile solvent can be followed by chemical reactions either of the remaining solid or, in the presence of high boiling co-solvents or molten salts, in submicron-sized liquid droplets. Such reactions can occur in the interior of the droplet or on the droplet surface. A very wide range of nanomaterials have been prepared by USP, including nanoporous metal oxides and sulfides, nanocomposites, very high surface area carbons, semiconductor quantum dots, and conductive metal inks.

Table 1. Characteristics of Various Nebulization Techniques.

Atomizer Type	Average Initial Droplet Size	Droplet Distribution	Gas Velocity	Droplet Delivery Rate
Ultrasonic (submerged)	1 to 10 μm	narrow	low	medium
Ultrasonic (nozzle)	10 to 1000 μm	medium	low	medium to high
Electrospray	<1 to 1000 μm	narrow	low	low to medium
Rotary	10 to 1000 μm	broad	low	high
Pressure	10 to 1000 μm	broad	high	high

Ultrasonic Nebulization and Aerosol Formation

In ultrasonic spray pyrolysis, ultrasound does not induce reactions such as those commonly found in sonochemical reactions,^{4,5} but instead generates a low-velocity aerosol.⁶ The ultrasound used for these techniques is typically low intensity and high frequency, ~2 MHz. The droplet formation by ultrasound was first described by R. W. Wood and A. L. Loomis in 1927, and in 1962, Lang experimentally established the relationship between ultrasonic frequency and average droplet size:

$$D_{\text{droplet}} = 0.34 \times \left(\frac{8\pi\gamma}{\rho f^2} \right)^{1/3}$$

where D_d is average droplet diameter, γ (N m^{-1}) is the liquid's surface tension, ρ (kg m^{-3}) is the solution density, and f (MHz) is the ultrasonic frequency.

Ultrasonic aerosol fountains (Figure 1A) are the result of capillary waves (i.e., waves travelling along the interface between two fluids) at the surface of liquids, and the aerosol generation is a result of momentum transfer. When the amplitude of the surface capillary waves is sufficiently high, the crests (peaks) of the waves can break off, resulting in liquid droplets. Since capillary wavelength is inversely proportional to wavelength, smaller droplets can be generated with higher frequencies.

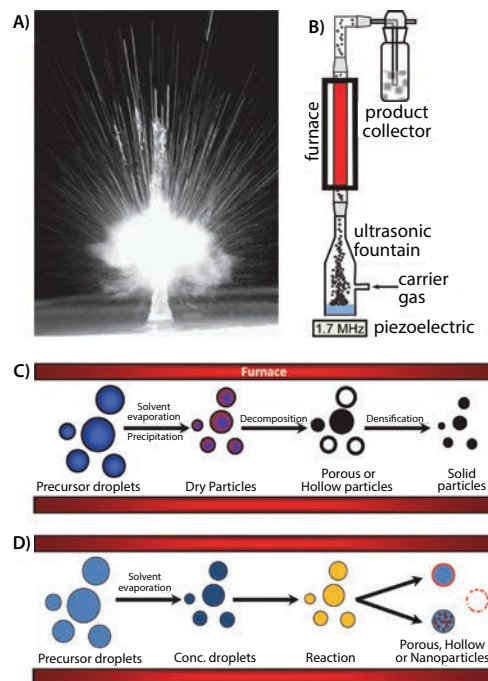


Figure 1. A) Photograph of an ultrasonic aerosol fountain produced using 1.7 MHz ultrasound. Schematic illustration of B) a typical laboratory scale USP apparatus, C) and D) simplified gas-solid USP and gas-liquid CAFS reaction processes, respectively.

USP and CAFS Apparatus

A typical USP reactor (Figure 1B) is composed of a high frequency ultrasonic transducer (like that found in a household humidifier) submerged in water below the base of a nebulization vessel containing the precursor solution. A thin, flexible polymer film (e.g. polyethylene, polypropylene, or polytetrafluoroethylene) is used at the base of the reactor reservoir to separate the precursor solutions from the ultrasonic transducer. This configuration allows ultrasound to be effectively transmitted through the polymer membrane into the precursor solution allowing nebulization to occur, while sequestering the solution under an inert or reactive gas of one's choosing. The nebulization vessel is fitted with a gas stream to carry the aerosol into a tubular furnace, and out to a collector (e.g., a bubbler, filter, electrostatic precipitator, etc.).

The USP process involves the sequence of (1) droplet generation, (2) evaporation of solvents in the heated zone, (3) diffusion of reactants, (4) reaction or precipitation, and (5) escape of any product volatiles. The nature of the final state is critically dependent on the phase of the material that remains after loss of the volatile solvent. USP has most commonly been used to produce solid particulates (i.e., spray drying) that may undergo solid state pyrolysis while in the tube furnace (Figure 1C). More recently, several groups have used high boiling co-solvents, ionic liquids, or molten salts to keep the droplets of the reacting aerosol in a liquid state throughout the heated zone; such droplets then serve as isolated micron-sized chemical reactors (Figure 1D). The use of liquid droplets has been referred to as salt-assisted^{7,8} USP or more generally, as chemical aerosol flow synthesis (CAFS).^{4,9-11}

Nanostructured Materials via Ultrasonic Spray Pyrolysis

Metal Oxides

Historically, the formation of metal oxides by USP has been heavily studied.^{2,12} By nebulizing precursor solutions containing water soluble metal salts (e.g. chloride, nitrate, acetate, hydroxides) or metal coordination complexes (e.g. peroxo-, ammonium, lactate, oxo-), a myriad of mono- and multi-metallic oxide powders have been created by USP. With the addition of polymers, colloidal silica, or other composites forming materials, new and complex architectures can be easily added to many of the simple oxide particles previously reported. For instance, utilizing an aqueous solution containing a titanium complex and colloidal silica, Suh and Suslick have prepared various forms of nanostructured titania (Figure 2).¹³⁻¹⁴ This combination of precursors produces porous titania microspheres after selectively etching the silica template with HF (Figure 2B). Interestingly, the addition of transition metal ions to the precursor solution caused an unusual phase separation to occur during USP, resulting in the outer shell becoming enriched in titania with the core of the particles consisting of silica. Etching the transition metal containing composites with HF for short periods of time yielded particles with a ball-in-ball morphology (Figure 2C), and further etching completely removed the silica leaving a hollow, porous titania spheres behind.¹⁴ Cytotoxicity studies revealed the microspheres had little effect on the viability of various cell lines. Further studies using these materials for delivery of a potent drug for the treatment of Alzheimer's disease (dehydroevodiamine) showed excellent selectivity for delivery to the cell cytosol rather than cell nuclei.¹⁵

Other examples of nanostructured oxide composites created by USP were pioneered by Okuyama and coworkers using polymer beads in the nebulized droplets as templates for creating macroporous oxide particles.¹⁶ One may expand upon this work by using inexpensive organic monomers (e.g., styrene), instead of expensive polymer beads, to generate interesting macroporous morphologies.¹³ One may also include $\text{Co}_2(\text{CO})_8$ (Aldrich Prod. No. 60811) in the precursor solution

to form ferromagnetic microsphere composites with nanoparticles of Co encapsulated in silica; these show no loss of magnetic susceptibility due to the oxidation of Co even after 6 months.¹³ More recently, the ultrasonic spray synthesis of oxides has been aimed at creating materials with specific applications, such as sensors for the detection of toxic industrial gases and photocatalysts for solar energy conversion.¹⁷ For example, chemically responsive inks, which have important applications to chemical sensing, have been made using a CAFS method by the condensation reaction of tetramethoxysilane (Aldrich Prod. Nos. 679259, 341436) and methyltrimethoxysilane (Aldrich Prod. No. 679232, 246174, 440175) around soluble dye molecules, producing an organically modified silica (ORMOSIL) pigment within the aerosol droplets.¹¹

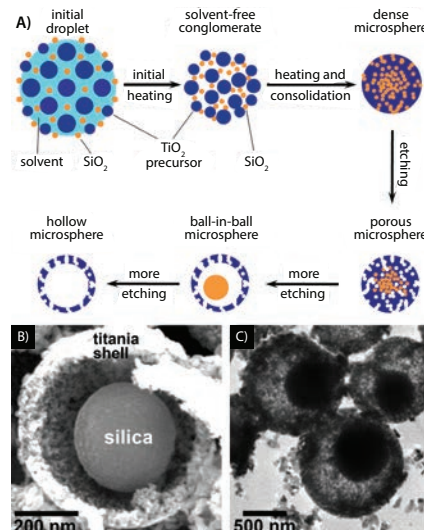


Figure 2. A) Schematic of the USP synthesis of porous, hollow, and ball-in-ball titania spheres, and electron micrographs of B) SEM and C) TEM images of ball-in-ball silica-titania composite decorated after partial etching with HF.

Metal Sulfides and Other Chalcogenides

While ultrasonic spray has proven to be a versatile route to many different oxide materials, a variety of nanostructured sulfides and other chalcogenides can be prepared using both USP and CAFS methods. For example, Skrabalak and Suslick,¹⁸ pyrolyzed aerosol solutions of $(\text{NH}_4)_2\text{MoS}_4$ (Aldrich Prod. No. 323446) and prepared a highly effective MoS_2 (Aldrich Prod. No. 234842, 69860) catalyst for hydrodesulfurization (HDS), the critical process for the removal of sulfur from petroleum. Porosity was induced in the MoS_2 microspheres by adding colloidal silica to the precursor solution and subjecting the material to a post-synthesis etching step (Figure 3). MoS_2 is a layered material with S-Mo-S---S-Mo-S layers; the catalytically active sites, however, are only the exposed Mo atoms at the edges of these layers. The nanoporosity induced by the silica template dramatically increases the number of active edge sites and the catalytic activity for hydrodesulfurization. When the porous MoS_2 was salt impregnated with Co as a promoter, the activity increased well above that of RuS_2 , which is known to be the most intrinsically active metal sulfide for the HDS process.

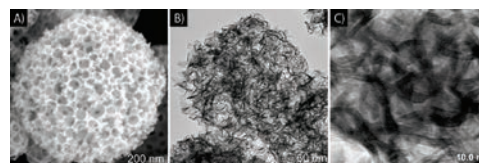


Figure 3. Porous MoS_2 , prepared by USP for catalytic hydrodesulfurization. A) SEM and B,C) TEM of porous MoS_2 .



CAFS has been used to prepare, on large scale, metal chalcogenide quantum dots (QDs).^{9,19} Didenko and Suslick developed a novel CAFS method using simple, low toxicity cadmium and chalcogenides precursors nebulized with a surfactant capping agent in a combination of toluene and high boiling point solvents (e.g., trioctylphosphine oxide). In this way, the individual droplets of solution act as reactors forming surfactant passivated CdS (Aldrich Prod. No. 662550), CdSe (Aldrich Prod. No. 662356), and CdTe (Aldrich Prod. No. 716669) QDs. Compared to prior batch processing, which use large volumes of high boiling point solvents into which aggressive and toxic chemicals must be injected quickly and reproducibly, the CAFS method provides a useful flow reactor alternative. The micron-sized droplets of the CAFS precursors are sufficiently small that fast, uniform heating occurs and high quality QDs are obtained as the volatile toluene co-solvent rapidly evaporates. The QDs prepared by CAFS were highly fluorescence with a quantum yield of ~25%, and were tunable over a broad spectra region by simply changing the temperature of the furnace.

Carbon Materials

Porous carbon materials are of interest for their potential use in electrochemical, catalytic, adsorbent, and gas-storage applications. Until recently, most porous carbons were prepared by carbonization of raw natural materials. Recent research efforts emphasize the use of templates and their subsequent removal to produce meso- and macroporous carbons with controlled, and in some cases, periodic pores. With this approach, a carbon precursor/inorganic template composite is first formed, followed by carbonization, then chemical leaching of the template material. Such methodology is tedious, requiring multiple synthetic steps, caustic chemical treatments, and long curing times; scale-up has also proven difficult and is not cost effective due to the destruction of (relatively) expensive templates.

CAFS provides an alternative approach for adding porosity, using molten salts within the droplets to form porous nanostructured carbon as reaction gases are released during the carbon formation. Skrabalak, Fortunato, and Suslick found that by nebulizing aqueous solutions of various organic salts (e.g. alkali metal chloroacetate and dichloroacetate) or even simple sugar mixed with alkali carbonate salts and pyrolyzing the aerosol droplets, they were able to create microspheres of carbon with diverse morphologies (Figure 4).²⁰⁻²¹ The choice of precursors is based on compounds in which a single carbon remains after the likely leaving groups (e.g., CO₂, HCl, H₂O) have been pyrolyzed away. These carbon materials have proved useful as catalyst supports in direct methanol fuel cells (DMFCs).²² By loading the porous carbons created by USP with catalysts consisting of PtRu (Aldrich Prod. No. 738573) and Pt (Aldrich Prod. Nos. 204013, 327441, 327476) alone for the anode and cathode, respectively, it was shown that the USP carbon microspheres could improve the electrical output of DMFCs when combined with traditional support materials in the anode and cathode.

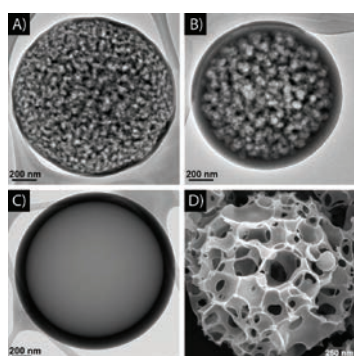


Figure 4. TEM images of carbons prepared by ultrasonic spray pyrolysis from 0.5 M sucrose and **A)** 1.0 M Na₂CO₃, **B)** 0.5 M Na₂CO₃, **C)** 0.5 M NaHCO₃, and **D)** 1.5 M sodium chloroacetate (H₂ClCCO₂Na). Furnace residence time is 9 s at 800 °C for A, B, and C, and 700 °C for D. These carbon materials have high surface areas (up to 800 m²/g) and very narrow pore size distributions.

Metals

USP can also be used to prepare metal nanoparticles and nanostructures for many precious and nonprecious metals, almost always by the use of metal oxides that decompose at temperatures below 1000 °C or by high temperature reduction with hydrogen in the flow gas.²³ Silver nanoparticles (of interest as printable conductive inks) (Aldrich Prod. No. 675318) have been made by Hong and coworkers using a liquid phase microreactor for the thermal reduction of silver pentafluoropropionate (Aldrich Prod. No. 326216) in isoamyl ether (Aldrich Prod. No. 260649) in the presence of trioctylamine²⁴ (Aldrich Prod. No. T81000) and a similar process was then scaled up using USP by Didenko and Ni.¹⁹ Forming highly reactive metal nanostructures (i.e., metals whose standard reduction potential is less than hydrogen) has remained a serious challenge, however, one that Helmich and Suslick recently addressed in a CAFS synthesis of metallic aluminum (Aldrich Prod. Nos. 518573, 653608).²⁵ Hollow, metallic aluminum particles were prepared by reacting trimethylamine aluminum hydride solution droplets with TiCl₄ (Aldrich Prod. Nos. 697079, 208566, 254312) vapor. Depending on the solution concentration and reaction temperature the morphology of the hollow microspheres could be changed from macroporous to nonporous. Ultrafine and nanoparticles of metallic aluminum have historically found use in propellants and pyrotechnics²⁶ and more recently as nanothermites.²⁷ The hollow morphology of the aluminum particles prepared by CAFS could easily be developed into similar applications.

Scale-Up and Industrial Applications

Ultrasonic spray pyrolysis on the laboratory scale at high frequencies (~2 MHz) as described earlier is very useful for rapid hypothesis testing and can easily prepare new and exotic materials on a small scale. The ultrasound intensity on the surface of the high frequency transducer, however, is not sufficient to atomize viscous, dense, or very high boiling solvents and slurries. In order to increase product throughput and spray larger amounts of liquid precursors, industrial scale setups for generation of small droplets of liquids using high intensity ultrasound are commercially available. Such ultrasonic nozzles work at frequencies from 20 to 120 kHz to create different droplet sizes (down to ~10 μm) and can spray up to ~100 mL/min of liquids with high viscosities, low vapor pressures and even slurries.¹⁹ An example of an industrial scale-apparatus equipped for ultrasonic spray pyrolysis is shown in Figure 5.

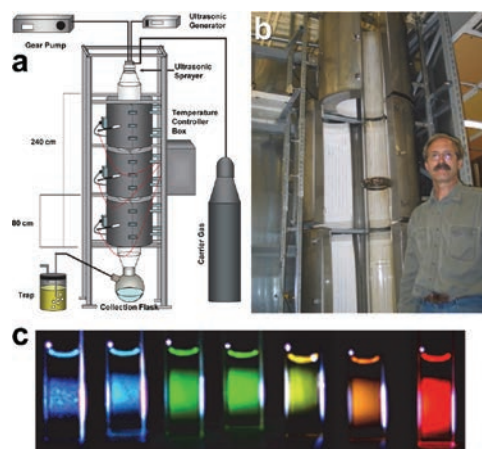


Figure 5. **A)** A pilot plant apparatus diagram with ultrasonic sprayer; **B)** photograph of the furnace with the inserted glass reactor (one of authors (Y.T.D., 6 ft tall) is shown for scale); **C)** fluorescence of CdSe quantum dots is controlled by particle size, which is tunable from 2 to 4 nm by use of the tube furnace temperature with fluorescence quantum yields of ~50%.



The yield and the quality of final products depends on the gas and liquid flow rates through the reactor, temperature inside the reactor, ultrasound power, solvents used and chemical composition of the mixture of precursors. By varying parameters of the experiments, it is possible to get very high yields. A variety of products can be obtained in this setup, including cadmium chalcogenide quantum dots (both core and core/shell), metal nanoparticles (silver, copper, nickel, copper/nickel and copper/silver alloys), and metal oxides. Many nanomaterials have been synthesized in a continuous-flow process using this apparatus.

The commercial market for quantum dots is currently dominated by biomedical applications and was worth of \$67 million in 2010 and is projected to grow to \$670 million by 2015.²⁸ Biomedical applications include bioimaging, flow cytometry, fluorescent labeling for cancer detection and intracellular imaging. The optoelectronics market for quantum dots is small at present, but likely to grow substantially with development of quantum dots for large scale industrial applications including solar energy harvesting, optical filters, displays, LEDs, etc.

The USP production of 10 nm silver nanoparticles (**Aldrich Prod. No. 730785**), and 4 nm gold nanoparticles have commercial applications as the base for high quality, inexpensive, low temperature sintering nanometallic inks, which opens the door for large-scale production of printable electronics as well as antimicrobial uses. The largest application of nanometals industrially is the nanosilver market, which is expected to grow from \$290 million in 2011 to ~\$1.2 billion in 2016.²⁹⁻³⁰ Nanosilver is used as an antibacterial material in filters for air and water purification, in textiles, and for wound treatment.³⁰⁻³¹ Other large scale applications of nanosilver include conductive nanoinks for printed circuits, front-side metallization of solar cells, thin film electronics, sensors, and catalysts. In addition, the market for other nanometals, such as gold, platinum and palladium may grow at an even higher rate than silver, specifically for biomedical applications.

As a final example, there are widespread and increasingly large markets for nanostructured metal oxides, from biomedical to photovoltaics and photocatalysts to lithium batteries.^{30, 32-33} Nanostructured silica, titania, iron oxides, zinc oxides, and a variety of binary/ternary metal oxides can all be produced via USP,¹²⁻¹⁶ and they have a variety of therapeutic applications and some are finding new applications in drug delivery formulations.³³⁻³⁵ Design of biodegradable and biocompatible nanocarriers based on these materials is under active development.^{31, 33-35}

Concluding Remarks and Future Outlook

Ultrasonic spray methods for preparing nanostructured materials have proven to be powerful tools and the revival of interest in USP over the past decade has been substantial. We have highlighted the diversity of applications and nanostructured materials accessible using ultrasonic spray methods. We expect that future work in this field will focus increasingly on the preparation of novel functional materials developed with specific purposes in mind (e.g., sorbents, catalyst and catalyst supports, sensors, and energetic materials) where the relationship between morphology and function can be readily pursued by exploring new precursors and aerosol synthetic routes.

Acknowledgments

This work was supported in part by the NSF DMR 09-06904, OII-0539385, IIP-0637721, and IIP-0823029. Materials characterizations were carried out in the Center for Microanalysis of Materials at the University of Illinois at Urbana-Champaign, which is partially supported by the U.S. DOE under grants DE-FG02-07ER46453 and DE-FG02-07ER46471.

References

- Hummel, R. E. *Understanding Materials Science: History, Properties, Applications*; 2nd ed.; Springer-Verlag: New York, 2004.
- Kodas, T. T.; Hampden-Smith, M. *Aerosol Processing of Materials*; Wiley-VCH: New York, 1999.
- Nandiyanto, A. B. D.; Okuyama, K. *Advanced Powder Technology* **2011**, *22*, 1.
- Bang, J. H.; Suslick, K. S. *Advanced Materials* **2010**, *22*, 1039.
- Suslick, K. S.; Price, G. *J. Annu. Rev. Mater. Sci.* **1999**, *29*, 295.
- Ashgriz, N. *Handbook of Atomization and Sprays: Theory and Applications*; Springer: New York, 2011.
- Xia, B.; Lenggono, W.; Okuyama, K. *Adv. Mater.* **2001**, *13*, 1579-1582.
- Okuyama, K.; Lenggono, W. *Chem. Eng. Sci.* **2003**, *58*, 537.
- Didenko, Y. T.; Suslick, K. S. *J. Am. Chem. Soc.* **2005**, *127*, 12196.
- Bang, J. H.; Suh, W. H.; Suslick, K. S. *Chem. Mater.* **2008**, *20*, 4033.
- Bang, J. H.; Lim, S. H.; Park, E.; Suslick, K. S. *Langmuir* **2008**, *24*, 13168.
- Messing, G. L.; Zhang, S.-C.; Jayanthi, G. V. *J. Am. Ceram. Soc.* **1993**, *76*, 2707.
- Suh, W. H.; Suslick, K. S. *J. Am. Chem. Soc.* **2005**, *127*, 12007.
- Suh, W. H.; Jang, A. R.; Suh, Y.-H.; Suslick, K. S. *Adv. Mater.* **2006**, *18*, 1832.
- Suh, W. H.; Suslick, K. S.; Suh, Y.-H. *Med. Chem. Cent. Nerv. Syst. Agents* **2005**, *5*, 259.
- Iskandar, F.; Mikrajuddin, A.; Okuyama, K. *Nano Lett.* **2002**, *2*, 389.
- Bang, J. H.; Helmich, R. J.; Suslick, K. S. *Adv. Mater.* **2008**, *20*, 2599.
- Skrabalak, S. E.; Suslick, K. S. *J. Am. Chem. Soc.* **2005**, *127*, 9990.
- Didenko, Y. T.; Ni, Y. "Controlled Synthesis of Nanoparticles Using Continuous Liquid-Flow Aerosol Method" US Patent 7,811,543 B2 issued 10/12/2010.
- Skrabalak, S. E.; Suslick, K. S. *J. Am. Chem. Soc.* **2006**, *128*, 12642.
- Fortunato, M. E.; Rostam-Abadi, M.; Suslick, K. S. *Chem. Mater.* **2010**, *22*, 1610.
- Bang, J. H.; Han, K.; Skrabalak, S. E.; Kim, H.; Suslick, K. S. *J. Phys. Chem. C* **2007**, *111*, 10959.
- Gürmen, S.; Stopic, S.; Friedrich, B. *Mater. Res. Bull.* **2006**, *41*, 1882.
- Xue, Z. L.; Terepka, A. D.; Hong, Y. *Nano Lett.* **2004**, *4*, 2227-2232.
- Helmich, R. J.; Suslick, K. S. *Chemistry of Materials* **2010**, *22*, 4835.
- Russel, M. S. *Chemistry of Fireworks*; RSC: Cambridge, 2009.
- Puszynski, J. A. *J. Therm. Anal. Calorim.* **2009**, *96*, 677.
- Oliver, J. *Quantum Dots: Global Market Growth and Future Commercial Prospects*; BCC Research: Wellesley, MA, 2011.
- Nanometals in Electronics and Energy Markets - 2012 and Beyond*. NanoMarkets.net, Glen Allen, VA, Dec. 21, 2011. http://nanomarkets.net/market_reports/report/nanometals_in_electronics_and_energy_markets_2012_and_beyond
- Evers, P. *Nanotechnology in Medical Applications: The Global Market*; BCC Research: Wellesley, MA, 2012.
- Li, Y. F.; Chen, C. Y. *Small* **2011**, *7*, 2965-2980.
- Ji, L. W.; Lin, Z.; Alcoutlabi, M.; Zhang, X. W. *Energy Environ. Sci.* **2011**, *4*, 2682-2699.
- Kumar, C. S. S. R. (ed.) *Nanostructured Oxides*; Wiley-VCH, Weinheim, 2009.
- Chandra, S.; Barick, K. C.; Bahadur, D. *Advanced Drug Delivery Reviews* **2011**, *63*, 1267-1281.
- Suh, W. H.; Suslick, K. S.; Stucky, G. D.; Suh, Y.-H. *Prog. Neurobiol.* **2009**, *87*, 133-170 <http://www.scs.illinois.edu/~suslick/documents/progneurobio.09133.pdf>.

Quantum Dots

For a complete list of available materials, visit aldrich.com/quantumdots

Name	Fluorescence Emission	Particle Size and λ_{abs}	Prod. No.
CdSe/ZnS quantum dots, 5 mg/mL in toluene/alipahtic amine	λ_{em} = 530 nm	-	731838-5ML 731838-25ML
CdSe/ZnS quantum dots, 5 mg/mL in toluene/alipahtic amine	λ_{em} = 590 nm	-	731846-5ML 731846-25ML
CdSe/ZnS quantum dots, 5 mg/mL in toluene/alipahtic amine	λ_{em} = 610 nm	-	731854-5ML 731854-25ML
CdSe/ZnS quantum dots, 5 mg/mL in toluene/alipahtic amine	λ_{em} = 485 nm	-	731862-5ML 731862-25ML
CdSe/ZnS quantum dots, 5 mg/mL in toluene/alipahtic amine	λ_{em} = 635 nm	-	731870-5ML 731870-25ML
Lumidot™ CdSe, 480, core-type quantum dots, 5 mg/mL in toluene, 480 core-type quantum dots	λ_{em} = 475-485 nm	~2.1 nm	662356-10ML
Lumidot™ CdSe, 520, core-type quantum dots, 5 mg/mL in toluene, 520 core-type quantum dots	λ_{em} = 515-525 nm	~2.5 nm	662437-10ML
Lumidot™ CdSe, 560, core-type quantum dots, 5 mg/mL in toluene, 560 core-type quantum dots	λ_{em} = 555-565 nm	~3.3 nm	662445-10ML
Lumidot™ CdSe, 590, core-type quantum dots, 5 mg/mL in toluene, 590 core-type quantum dots	λ_{em} = 585-595 nm	particle size 4.0 - 4.3 nm	662607-10ML
Lumidot™ CdSe, 610, core-type quantum dots, 5 mg/mL in toluene, 610 core-type quantum dots	λ_{em} = 605-615 nm	~5.0 nm	662488-10ML
Lumidot™ CdS, 380, core-type quantum dots, 5 mg/mL in toluene, 380 core-type quantum dots	λ_{em} = 370-390 nm	~2.3 nm	662429-10ML
Lumidot™ CdS, 460, core-type quantum dots, 5 mg/mL in toluene, 460 core-type quantum dots	λ_{em} = 450-470 nm	~5.0 nm	662372-10ML
Lumidot™ CdS, 480, core-type quantum dots, 5 mg/mL in toluene, 480 core-type quantum dots	λ_{em} = 470-490 nm	~5.6 nm	662364-10ML
Lumidot™ CdS-6, quantum dot nanoparticles kit, core-type, core-type	λ_{em} = 380-480 nm	-	662593-1KT

Nanoparticles and Inks

For a complete list of available materials, visit aldrich.com/nanomaterials

Name	Composition	Concentration	Particle Size and λ_{abs} and λ_{em}	Prod. No.
Silver, dispersion	Ag	0.02 mg/mL in aqueous buffer, sodium citrate as stabilizer	particle size 40 nm (TEM) / 412 nm	730807-25ML
Silver, dispersion	Ag	0.02 mg/mL in aqueous buffer sodium citrate as stabilizer	particle size 20 nm (TEM) / 401 nm	730793-25ML
Silver, dispersion	Ag	0.02 mg/mL in aqueous buffer sodium citrate as stabilizer	particle size 10 nm (TEM) / 388 nm	730785-25ML
Silver nanoparticle ink	Ag	20 wt. % (dispersion in organic solvents) in ethanol and ethanediol	particle size <150 nm (DLS)	719048-5ML 719048-25ML
Silver	Ag	solids 70-80%	-	735825-25G
Gold nanoparticles	Au	~ 7.8E+9 particles/mL	diameter 80 nm, $\lambda_{abs}/\lambda_{max}$ 551-557 nm	742023-25ML 742023-100ML
Gold nanoparticles	Au	~ 1.9E+10 particles/mL	diameter 60 nm, $\lambda_{abs}/\lambda_{max}$ 538-544 nm	742015-25ML 742015-100ML
Gold nanoparticles	Au	~ 5.5E+13 particles/mL	diameter 5 nm, $\lambda_{abs}/\lambda_{max}$ 510-525 nm	741949-25ML 741949-100ML
Gold nanoparticles	Au	~ 7.2E+10 particles/mL	diameter 40 nm, $\lambda_{abs}/\lambda_{max}$ 529-533 nm	741981-25ML 741981-100ML
Gold nanoparticles	Au	~ 7.2E+11 particles/mL	diameter 20 nm, $\lambda_{abs}/\lambda_{max}$ 518-522 nm	741965-25ML 741965-100ML
Gold nanoparticles	Au	~ 6.0E+12 particles/mL	diameter 10 nm, $\lambda_{abs}/\lambda_{max}$ 510-525 nm	741957-25ML 741957-100ML

Common Precursors for Ultrasonic Spray Pyrolysis

For a complete list of available materials, visit aldrich.com/periodic

Name	Composition	Purity	Description	Prod. No.
Lithium carbonate	Li_2CO_3	99.999%	powder	752843-25G
Sodium bromide hydrate	$\text{NaBr}\cdot\text{H}_2\text{O}$	99.999% trace metals basis	solid	751952-5G
Sodium nitrate, anhydrous	NaNO_3	99.995% trace metals basis	solid	757586-5G
Sodium carbonate, anhydrous	Na_2CO_3	99.999% trace metals basis	powder	451614-5G 451614-25G 451614-50G
Sodium carbonate decahydrate	$\text{Na}_2\text{CO}_3 \cdot 10\text{H}_2\text{O}$	99.999% trace metals basis	crystalline	577782-250G 577782-1KG
Aluminum(III) fluoride, anhydrous	AlF_3	99.999%	solid	752983-5G
Aluminum acetate, basic	$\text{C}_7\text{H}_9\text{O}_4\text{Al}$	-	powder	294853-250G 294853-1KG
Aluminum isopropoxide	$\text{Al}[\text{OCH}(\text{CH}_3)_2]_3$	≥99.99% trace metals basis	powder and chunks	229407-10G 229407-50G 229407-250G
Potassium carbonate, anhydrous	K_2CO_3	99.99% trace metals basis	powder	590681-5G 590681-25G



Name	Composition	Purity	Description	Prod. No.
Titanium(II) chloride, anhydrous	TiCl ₂	99.98% trace metals basis	powder	451738-1G 451738-5G
Titanium(III) chloride-aluminum chloride	(TiCl ₃) ₃ · AlCl ₃	-	solid	456411-50G
Titanium(III) oxide	Ti ₂ O ₃	99.9% trace metals basis	powder, -100 mesh	481033-10G 481033-50G
Cobalt(II) chloride, anhydrous	CoCl ₂	99.999% trace metals basis	beads, -10 mesh	409332-1G 409332-5G
Cobalt(II) oxide	CoO	≥99.99% trace metals basis	powder	529443-5G 529443-25G
Cobalt(II) nitrate hexahydrate	Co(NO ₃) ₂ · 6H ₂ O	99.999% trace metals basis	crystals and lumps	203106-10G 203106-50G
Cobalt(II) carbonate hydrate	CoCO ₃ · xH ₂ O	99.998% trace metals basis	powder	379956-5G
Cobalt(II) acetate tetrahydrate	(CH ₃ COO) ₂ Co · 4H ₂ O	99.999% trace metals basis	powder and chunks	437875-1G 437875-10G
Cobalt(II) acetate	(CH ₃ CO ₂) ₂ Co	99.995% trace metals basis	powder or crystals	399973-1G 399973-10G
Bis(cyclopentadienyl)cobalt(II)	Co(C ₅ H ₅) ₂	-	powder or crystals	339164-2G 339164-10G
Nickel(II) chloride hexahydrate	NiCl ₂ · 6H ₂ O	99.9% trace metals basis	solid	654507-5G 654507-25G 654507-100G
Nickel(II) oxide	NiO	99.999% trace metals basis	solid	481793-5G 481793-25G
Nickel carbonate, basic hydrate	NiCO ₃ · 2Ni(OH) ₂ · xH ₂ O	99.9% trace metals basis	powder	544183-250G-A 544183-1KG-A
Nickel(II) acetate tetrahydrate	Ni(OCOCH ₃) ₂ · 4H ₂ O	99.998% trace metals basis	powder and chunks	379883-10G 379883-50G
Copper(II) chloride	CuCl ₂	99%	powder	751944-25G
Copper(I) chloride, anhydrous	CuCl	≥99.99% trace metals basis	beads	651745-5G 651745-25G
Copper(I) bromide	CuBr	99.99% trace metals basis	beads, -10 mesh	735906-25G
Copper(I) oxide, anhydrous	Cu ₂ O	≥99.99% trace metals basis	powder	566284-5G 566284-25G
Copper(II) nitrate hemi(pentahydrate)	Cu(NO ₃) ₂ · 2.5H ₂ O	≥99.99% trace metals basis	crystalline	467855-50G 467855-250G
Copper(II) acetylacetonate	Cu(C ₅ H ₇ O ₂) ₂	≥99.99% trace metals basis	powder	514365-10G 514365-50G
Molybdenum(V) chloride, anhydrous	MoCl ₅	99.99% trace metals basis	powder	642452-2G 642452-10G
Molybdenum(III) chloride	MoCl ₃	99.95% trace metals basis	powder	339334-2G
Molybdenum(IV) oxide	MoO ₂	97%	powder	711209-10G 711209-50G
Molybdenum(VI) oxide	MoO ₃	99.99% trace metals basis	powder	203815-5G 203815-25G
Molybdenum(VI) tetrachloride oxide	MoOCl ₄	-	powder or crystals	373729-5G 373729-25G
Molybdenum(II) acetate dimer	Mo ₂ (OCOCH ₃) ₄	98%	needles	232076-250MG 232076-1G 232076-5G
Molybdenumhexacarbonyl	Mo(CO) ₆	≥99.9% trace metals basis	solid	577766-5G 577766-25G
Cadmium chloride hydrate	CdCl ₂ · xH ₂ O	99.995% trace metals basis	solid	529575-10G 529575-50G
Cadmium oxide	CdO	≥99.99% trace metals basis	powder	202894-5G 202894-25G
Cadmium nitrate tetrahydrate	Cd(NO ₃) ₂ · 4H ₂ O	98%	solid	642045-100G 642045-500G
Cadmium carbonate	CdCO ₃	98%	powder, 1 μm	289140-100G 289140-500G
Cadmium hydroxide	Cd(OH) ₂	99.99% trace metals basis	powder	401560-1G
Cadmium(II) acetate, anhydrous	Cd(OCOCH ₃) ₂	99.995%	solid	755087-5G
Silver nitrate	AgNO ₃	99.9999% trace metals basis	crystalline	204390-1G 204390-10G 204390-50G 204390-250G
Silver acetate	CH ₃ COOAg	99.99% trace metals basis	powder or crystals	204374-10G 204374-50G
Silver acetylacetonate	[CH ₃ COCH=C(O)CH ₃] ₂ Ag	98%	solid	323489-1G 323489-5G

Physical Vapor Deposition

Sputtering Targets, Evaporation Slugs and Metal Foils

Today, Physical Vapor Deposition (PVD) technique is used in a variety of applications, including fabrication of microelectronic devices, interconnects, flat panel displays, photovoltaics, battery and fuel cell electrodes, diffusion barriers, optical and conductive coatings, and surface modifications. PVD is a vacuum deposition process used to deposit thin layers of materials, in the range of few nanometers to several micrometers.

Selected Circular Sputtering Targets (purity, trace metals basis)

- Aluminum 99.9995% ([Prod. No. 749036](#))
- Titanium 99.995% ([Prod. No. 749044](#))
- Zinc oxide 99.99% ([Prod. No. 752681](#))
- Indium tin oxide 99.99% ([Prod. No. 752657](#))

Selected Evaporation Slugs (purity, trace metals basis)

- Iridium 99.9% ([Prod. No. 449229](#))
- Titanium $\geq 99.99\%$ ([Prod. No. 433675](#))
- Platinum 99.99% ([Prod. No. 373230](#))
- Palladium 99.95% ([Prod. No. 373206](#))

Selected Metal Foils (purity, trace metals basis)

- Aluminum 99.999% ([Prod. No. 266957](#))
- Cadmium $\geq 99.99\%$ ([Prod. No. 265411](#))
- Cobalt $\geq 99.99\%$ ([Prod. No. 266671](#))
- Copper 99.999% ([Prod. No. 266744](#))
- Gold 99.99% ([Prod. No. 265829](#))

Custom designed materials, including metal filled crucibles for Molecular Beam Epitaxy (MBE), are also available through our **Hard Materials Center of Excellence**. To inquire, please contact hardmaterials@sial.com.

Aldrich Materials Science offers a variety of high purity materials for PVD techniques.

For complete list of materials and detailed product information, visit

aldrich.com/pvd





Advanced Inorganic Materials for Solid State Lighting



Alexander Birkel,¹ Kristin A. Denault,^{2,3} Nathan C. George,⁴ and Ram Seshadri^{1,2,3*}
¹Mitsubishi Chemical Center for Advanced Materials,
²Solid State Lighting and Energy Center,
³Materials Department, and ⁴Department of Chemical Engineering,
 University of California, Santa Barbara, CA 93106
 *Email: seshadri@mrl.ucsb.edu

A Bright Future for Solid-State Lighting

In 1907, the first electroluminescent device, with silicon carbide (Aldrich Prod. Nos. 594911, 378097, 357391) as the active material, was described by Henry Round as displaying a "bright glow".^{1,2} Lighting based on solid-state devices has since come a long way. The development of bright "candela-class" green, blue, and near-UV diodes by Nakamura³ in the 1990s was a major breakthrough, completing the spectral gamut of white light and allowing solid state lighting (SSL) to develop into a viable alternative to other, lower-efficiency light sources, such as incandescent bulbs and even compact fluorescent lamps (CFL). Offering higher efficiencies, longer lifetimes (50,000 to 100,000 hours, compared to up to 15,000 for CFLs and only 1,000 - 2,000 for incandescent light bulbs), and the absence of toxic elements such as mercury, SSL is on the verge of becoming the standard technology for artificial light sources.⁴⁻⁶

White solid-state light can be generated using three different approaches: By employing three diodes that emit red, green and blue light respectively, by using a near-UV LED that excites several phosphors that emit over the complete spectral range, or the third, most widely used alternative entailing down-conversion of a portion of blue LED light to longer wavelengths in such a manner that white light emerges. The other strategies are less used due to certain intrinsic difficulties. For example, LEDs that efficiently emit in the green region of the visible spectrum cannot currently be produced and this holds back the three-LED strategy, and the near-UV with full down-conversion strategy is intrinsically inefficient due to the large Stokes shifts involved. Inorganic phosphors play a key role in carrying out the widely employed partial down-conversion strategy.⁷

Phosphors provide the necessary green/yellow/red light needed, in addition to the originally emitted blue, for a white light source. Inorganic phosphors usually consist of a host crystal that could be an oxide, oxynitride, nitride, halide or oxyhalide selected for their wide band gaps and other key features, doped with a small amount of rare earth and/or transition metal ions that act as the emissive center.⁸⁻¹² As shown in the *CIE* (Commission Internationale de l'Éclairage) diagram in Figure 1, virtually every color can be rendered with the use of inorganic luminescent materials in combination with a near-UV or blue light source.

Phosphors can be prepared using the rare earth ions such as Eu^{3+} , Tb^{3+} or Sm^{3+} . However, in these systems, the emission relies on f to f transitions which are parity forbidden and therefore rather inefficient. In addition, the lower lying f -orbitals are rather well-shielded from the coordination environment of the ion and, consequently, the emission arising from those f - f transitions are sharp and not very suitable for

covering a large region of the visible spectrum. To circumvent these issues of narrow, inefficient emission, the most frequently used phosphors are doped with broad-emitting ions, such as Mn^{2+} , Ce^{3+} , or Eu^{2+} (see also the examples in Figure 1). In the case of Ce^{3+} and Eu^{2+} , light is emitted due to $4f$ to $5d$ transitions within the ion. In the free Ce^{3+} ion, the $5d$ states are degenerate and lie at a much higher energy above the two $4f$ ground states of the ion. However, d -orbitals have a pronounced interaction with the crystalline lattice, as indicated in Figure 2 for the case of Ce^{3+} . Once introduced into a host lattice, the energy levels of the d -orbitals are reduced due to their interactions with the surrounding ligands (centroid shift due to the nephelauxetic effect). The crystal field splitting, due to the varying interactions of the ligands with the different (xy , xz , yz , x^2-y^2 , z^2) d -orbitals, lifts the degeneracy and, in most structures, leads to as many as five states distinct in energy. The difference in energy between the d -states in the free ion and the lowest lying d -state in the crystalline host is called $D(A)$, or the spectroscopic red-shift.¹³

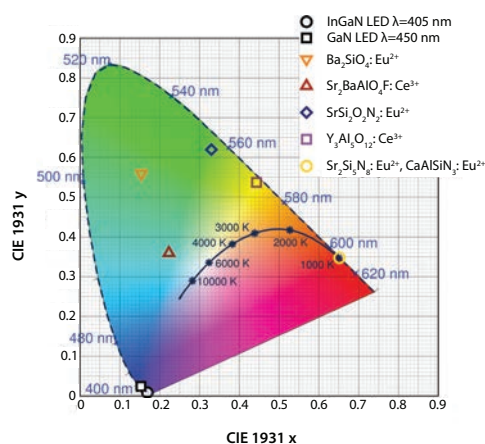


Figure 1. Color coordinates of some phosphor materials, and of blue and near-UV LEDs.

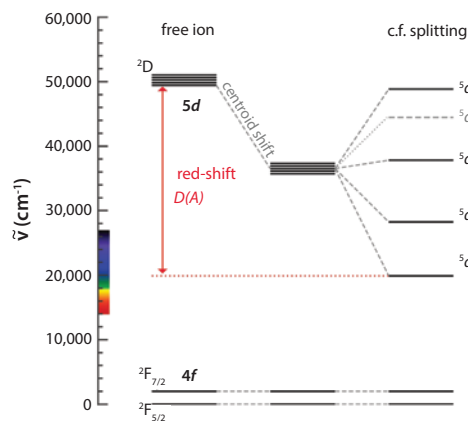


Figure 2. Electronic states of the free cerium ion and the crystal field splitting that is observed in host matrices.⁵



The Quest for Improved Materials

As a consequence of being so crucial for SSL, significant research efforts have been expended on the development of new phosphor materials. A schematic representation of this type of solid-state white lighting device is shown in **Figure 3**. It consists of a blue-emitting LED chip with the phosphor directly above the chip, dispersed in a transparent silicone¹², or in form of a cap, as shown in **Figure 3**. The blue light passes through this phosphor layer that converts part of the blue light to yellow, which yields (cool) white light. There are many issues of efficiency (many phosphors do not possess near 100% quantum efficiency), appropriate color rendition, and color temperature that drive phosphor research. Also important is loss of efficiency at elevated temperatures that is becoming increasingly relevant to higher-power LED white light sources, such as those used in the front-lighting of automobiles.

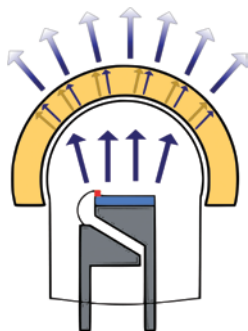


Figure 3. Representation of the generation of white light by emission of blue light from a LED, which is then down-converted by a yellow phosphor encapsulated in silicone resin cap.

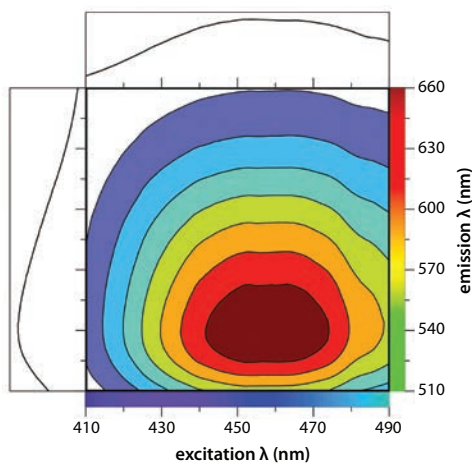


Figure 4. The 2D excitation/emission spectra of $\text{Y}_3\text{Al}_5\text{O}_{12}:\text{Ce}^{3+}$. The excitation band shows a maximum around 460 nm, whereas the emission maximum is located at around 550 nm. The 1D excitation/emission spectra are shown on the left and top of the figure, and were taken using the emission/excitation wavelengths corresponding to the maximum intensity in the spectra.

In order to achieve the best possible device efficiency, phosphors need to fulfill certain requirements, which include, but are not limited to:

1. A very high quantum efficiency, in order to maximize the number of photons that are (re)-emitted by the phosphors.
2. A suitable excitation and emission spectrum. The excitation spectrum of the phosphor should possess considerable spectral overlap with the emission spectrum of the LED in order for efficient pumping to be achieved. An example is presented in **Figure 4**, showing the emission and excitation spectrum of cerium-doped $\text{Y}_3\text{Al}_5\text{O}_{12}$ (YAG) (Aldrich Prod. No. 634638). The emission of the phosphor itself should be broad, thus well reproducing the wide spectral gamut of the sun. This property is measured as the color-rendering index, CRI or R_a , which compares the color rendering of any light source to a reference black body source at temperatures near 5000 K. Values of 90 or more are desirable.
3. Excellent device and color stability in regards to both chemical and thermal factors. This is important for the long term prospects of solid state lighting devices. It is also important for the use of phosphors on high power LED chips, which can reach temperatures of nearly 200 °C under operation.

Often, some of those requirements are conflicting. This means that, for example, broad emitting phosphors might possess a poor efficiency, while materials with suitable quantum efficiency may not cover the desired wavelength range with their emission spectrum. Some of those properties are strongly dependent on the dopant ion, whereas others are easily influenced by the host matrix. The challenge for materials scientists is thus to find the optimum combination of host lattice and activator ion(s) to eventually prepare stable, inexpensive, and efficient materials.

Phosphor Preparation

Various preparative methods have been developed to obtain phase-pure and high-quality phosphor materials. Usually, high temperature solid-state reactions are the method of choice, meaning that the starting compounds (typically oxides, carbonates, or nitrates) are thoroughly mixed and homogenized and then subsequently heated at temperatures usually ranging from 1000 °C to 1600 °C. Reducing atmospheres, such as mixtures of H_2 and N_2 or CO gas, are often used in order to convert the dopant ion to the desired valence state (e.g., Ce^{3+} instead of Ce^{4+} , and Eu^{2+} instead of Eu^{3+}). Alternative reactions include solution-based approaches such as hydro- or solvothermal preparations, or sol-gel and spray pyrolysis methods.

More exotic synthetic pathways include combustion syntheses, as well as microwave-assisted solid state preparations,¹⁴ that offer unmatched reaction speeds, but much less control of the properties of the final product. The preparation of oxynitrides and nitrides often requires harsher conditions, such as very high temperatures (sometimes more than 2000 °C) and high N_2 partial pressures in order to ensure incorporation of the nitrogen into the crystal lattice. Usually, air-sensitive precursors call for preparation steps under inert conditions, which is also true for some oxide materials.

Oxide Phosphors

Among the many different phosphor hosts that have been investigated, oxides have the largest share due to their ease of preparation and low cost production, often combined with excellent stability of the resulting compounds. By far the most widely used material in solid state lighting today is yttrium aluminum garnet, $Y_3Al_5O_{12}$, doped with small amounts of cerium, abbreviated as YAG:Ce. The most efficient materials are prepared at temperatures above 1500 °C and are typically doped with 2 mol-% to 3 mol-% of cerium. An image of the unit cell is presented in **Figure 5A**. YAG crystallizes in a cubic space group $Ia-3d$ and it consists of AlO_4 tetrahedra and AlO_6 octahedra that are completely corner-connected and form a stiff, highly connected three-dimensional network.

Y^{3+} ions occupy the voids within this network and these are coordinated by a total of eight oxygen ions, forming a distorted coordination environment. The Y^{3+} ions are also connected in three dimensions by their polyhedral edges, forming an intertwining network with the connected AlO_n polyhedra in the manner of double gyroid structures known in block copolymers. First prepared by Blasse and Bril in 1967,¹⁵ YAG:Ce has become the canonical phosphor material in solid state white lighting applications. The reasons are manifold. Consisting only of relatively inexpensive and abundant elements, it can be prepared in large scales at a low cost. The optical properties make it a very good phosphor material as well. YAG:Ce shows a broad excitation band around 450 nm, making it a perfect fit for the emission of blue InGaN LEDs. The broad emission band of YAG:Ce is centered at around 550 nm, but reaches as far 650 nm (see **Figures 1 and 4**), creating the aforementioned cool white light in conjunction with a blue light emitting diode.¹⁶

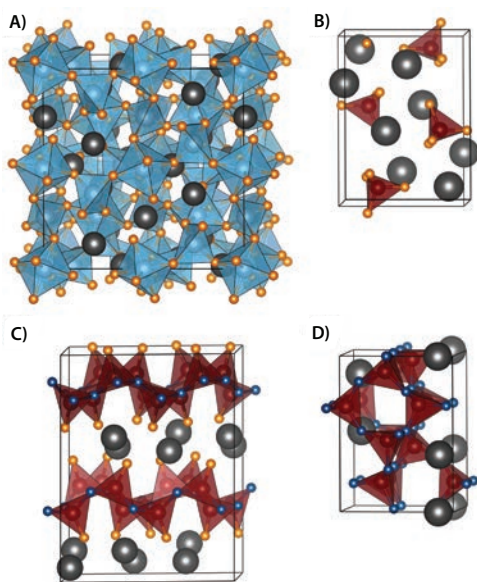


Figure 5. Schematic depictions of the unit cells of widely used phosphors. Here, **A)** shows the garnet $Y_3Al_5O_{12}$, **B)** the orthosilicate Ba_2SiO_4 , **C)** the oxynitride $CaSi_2O_2N_2$ and **D)** the nitride $Sr_2Si_2N_6$. Grey spheres represent Y, Ba, Ca and Sr atoms, while light blue, red, orange, and dark blue spheres represent Al, Si, O, and N atoms, respectively.

Additionally, it boasts several other very desirable properties, such as very good chemical and temperature stability. This is an important issue in phosphor-converted solid state lighting. Although much more electrical energy is transformed into visible light than in other lighting devices, the LED chip, which emits the radiation that eventually excites the phosphor, can reach temperatures of several hundred degrees Celsius. As shown in **Figure 6**, the emission wavelength of YAG:Ce does not change significantly with increasing temperature and the quantum efficiency drops only slightly below the value at room temperature, thus making long-term lighting applications feasible.

Also, the emission wavelength of cerium-doped YAG can somewhat be tuned by modifying its chemical composition (e.g., - substituting Y^{3+} by Gd^{3+} , Lu^{3+} , and the Al^{3+} by combinations of Mg^{2+} and Ge^{4+}/Si^{4+}). The change in the chemical composition leads to differences in the coordination environment of the emitting ion due to variations in the bond lengths or the strength and type of those bonds, thus modifying the crystal field splitting. Of course, the anionic composition can also be modified, as we will address later in the case of (oxy)nitrides. This chemical tuning of the emission wavelength of a phosphor is an important tool for the materials scientist.

Changes in composition play a very important role in another vast class of oxide phosphor materials, the orthosilicates. Possessing a very rich chemistry (almost 90% of the earth's crust consists of silicates), some silicates, if doped with broad emitting ions (Ce^{3+} , Eu^{2+}), are remarkable phosphor materials that exhibit high quantum efficiency and good temperature stability. Here, we would like to briefly discuss the structure and properties of one of the simplest members of the phosphor silicate family, barium orthosilicate, Ba_2SiO_4 . As its systematic name tells, the structure of Ba_2SiO_4 (orthorhombic space group $Pnma$) is composed of $[SiO_4]^{4-}$ tetrahedra that are isolated from one another (thus *orthosilicate*), as shown in **Figure 5B**. The Ba^{2+} ions in this structure occupy two distinct crystallographic sites and are either 9- or 10-fold coordinated. Due to the uncomplicated synthesis (high temperature route in reducing atmospheres) and because of the ability to form solid-solutions with the strontium and calcium end members, phosphors from the orthosilicate family, especially the barium compounds, have been the focus of many research efforts.

The introduction of small amounts of europium ions leads to strong green emission (maximum centered around 505 nm) under near-UV (~395 nm) excitation (see also the color coordinates in **Figure 1**).¹⁷ This very intense emission in the green part of the spectrum makes it a suitable candidate for white light generation that relies on multiple color phosphors or phosphor blends.

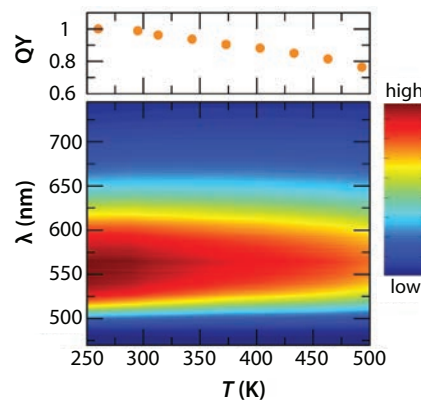


Figure 6. Temperature-dependence of the emission properties and the photoluminescence quantum yield of $Y_3Al_5O_{12} : Ce^{3+}$.

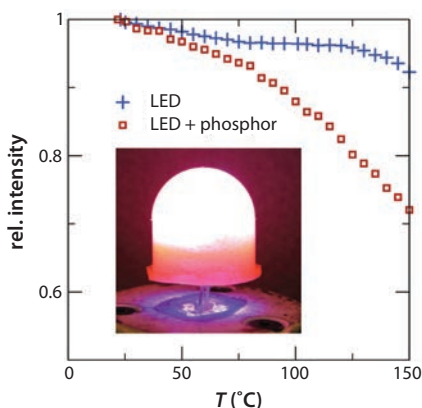


Figure 7. The relative intensity decrease of the $\text{Sr}_2\text{Si}_5\text{N}_8:\text{Eu}^{2+}$ phosphor and LED with increasing temperature shows the high thermal stability of this phosphor, uncommon among other red emitting phosphors. The inset shows a photograph of the phosphor encapsulated silicone cap illuminated by a blue LED.²²

(Oxy)nitride Phosphors

As briefly mentioned earlier, one possibility to tune the emission color (among other properties) is through the chemical substitution of either the cations or the anions. Another class of phosphors that is related to orthosilicates are oxynitrides from the family $M\text{Si}_2\text{O}_2\text{N}_2:\text{Ln}$, where M is Ca, Sr or Ba and Ln is Ce^{3+} or Eu^{2+} .^{18,19} A depiction of the unit cell of $\text{CaSi}_2\text{O}_2\text{N}_2$ is shown in **Figure 5C**. It consists of alternating layers of Ca^{2+} ions and layers formed by a network of SiON_3 tetrahedra that are connected *via* the three nitrogen terminated corners. The structures of the Sr and Ba $M\text{Si}_2\text{O}_2\text{N}_2:\text{Ln}$ oxynitrides are similar, however the difference in composition results in slightly different unit cell dimensions. Exhibiting high quantum efficiencies (up to 93% at room temperature) and very good temperature stability (quenching temperatures as high as 600 K for $\text{SrSi}_2\text{O}_2\text{N}_2$ and $\text{BaSi}_2\text{O}_2\text{N}_2:\text{Eu}^{2+}$), these compounds and solid solutions thereof have quickly become well-studied and widely-used as alternative down-converting materials for white light emitting devices. If doped with divalent europium, the emission maxima of the pure compounds (*i.e.* $\text{CaSi}_2\text{O}_2\text{N}_2$, $\text{SrSi}_2\text{O}_2\text{N}_2$, $\text{BaSi}_2\text{O}_2\text{N}_2$) is centered around 558 nm, 538 nm and 495 nm, respectively. Compositional tuning between these end members has led to very efficient yellow-green phosphors which are potentially substitutes for YAG:Ce.

A fourth class of phosphors is nitrides, which often have a red-shifted emission color when compared to oxides. The red shift is due to the large nephelauxetic effect in nitrides, which decreases the Racah interelectronic repulsion parameter of the activator ion and results in large crystal field splittings. Red emission from lighting is crucial for lowering the color temperature of lighting, making solid state lighting sources more pleasing to the eye and suitable for residential lighting applications. A well-known example of nitride phosphors is the family $M_2\text{Si}_5\text{N}_8:\text{Ln}$, where M is Sr or Ba and Ln is Ce^{3+} or Eu^{2+} .^{20,21} The structure is orthorhombic (space group $Pmn2_1$), shown for $\text{Sr}_2\text{Si}_5\text{N}_8$ in **Figure 5D**. The unit cell consists of a fully connected network of corner sharing SiN_4 tetrahedra, which extends in all three dimensions. The Sr^{2+} ions sit in the voids created by the SiN_4 network, resulting in two distinct sites that are 6- and 7-fold coordinated. A complete solid solution can be formed with 100% Eu^{2+} substitution for Sr or Ba. Substitution of Eu^{2+} results

in red emission from $\text{Sr}_2\text{Si}_5\text{N}_8$ and yellow emission from $\text{Ba}_2\text{Si}_5\text{N}_8$, while increasing amounts of Eu^{2+} red shift the emission to a maximum of 680 nm. The highly interconnected lattice of $\text{Sr}_2\text{Si}_5\text{N}_8$ results in high quantum efficiency (up to 80% at room temperature) and very good thermal stability for a red emitting phosphor as shown in **Figure 7**.²² The excitation band of $\text{Sr}_2\text{Si}_5\text{N}_8:\text{Eu}^{2+}$ ranges from 370 nm to 460 nm and this, in addition to the highly efficient and stable red emission, make this compound an attractive choice for a conversion phosphor to add a red spectral component to InGaN-based warm white LEDs.

Summary

Solid-state lighting offers a potential for great energy savings. The performance of solid-state lighting devices critically depends on the down-converting phosphor or combination of phosphors used in the device. As we have shown, advanced inorganic materials including, but not limited to, oxides, oxynitrides and nitrides doped with small amounts of rare earth and/or transition metal elements, can be used as phosphors to efficiently create white light in a solid-state device.

Acknowledgements

We gratefully acknowledge support for work in the solid state lighting area from the Mitsubishi Chemical Center for Advanced Materials, and the Solid State Lighting and Energy Center at UC Santa Barbara, and would like to thank Steve DenBaars, Shuji Nakamura, and Glenn Fredrickson. We thank Stuart Brinkley and Alexander Mikhailovsky for their many collaborations. KAD and NCG gratefully acknowledge the NSF ConvEne IGERT Program (NSF-DGE 0801627) for fellowship support.

References

- (1) Round, H. J. *Electr. World* **1907**, 49, 308.
- (2) Zheludev, N. *Nature Photon.* **2007**, 1, 189-192.
- (3) Nakamura, S.; Mukai, T. and Senoh, M. *Appl. Phys. Lett.* **1994**, 64, 1687-1689.
- (4) Ye, S.; Xiao, F.; Pan, YX.; Ma, YY.; and Zhang, QY. *Mater. Sci. and Eng. R* **2010**, 71, 1-34.
- (5) Smet, P.F.; Parmentier, A.B.; and Poelman, D. *J. Electrochem. Soc.* **2011**, 158 (6), R37-R54.
- (6) Pimputkar, S.; Speck, J.S.; DenBaars, S.P.; Nakamura, S. *Nature Photon.* **2009**, 3, 2-4.
- (7) Crawford, M. D. *J. Sel. Top. Quant.* **2009**, 15, 1028-1040.
- (8) Im, W. B.; Fellows, N. N.; DenBaars, S. P.; Seshadri, R. *J. Mater. Chem.* **2009**, 19, 1325.
- (9) Li, Y. Q.; Delsing, A. C. A.; With, G. D.; Hintzen, H.T. *Powder Diffr.* **2005**, 3242-3248.
- (10) Hecht, C.; Stadler, F.; Schmidt, P. J.; Baumann, V.; Schnick, W. *Chem. Mater.* **2009**, 21, 1595-1601.
- (11) Im, W.B.; George, N.; Kurzman, J.; Brinkley, S.; Mikhailovsky, A.A.; Hu, J.; Chmelka, B.F.; DenBaars S.P.; Seshadri, R. *Adv. Mater.* **2011**, 23, 2300-2305.
- (12) Im, W.B.; Brinkley, S.; Hu, J.; Mikhailovsky, A.A.; DenBaars S.P.; Seshadri, R. *Chem. Mater.* **2010**, 22, 2842-2849.
- (13) Dorenbos, P. *Phys. Rev. B.* **2000**, 62, 15640-15649.
- (14) Birkel, A.; Denault, K.A.; George, N.C.; Doll, C.; Héry, B.; Mikhailovsky, A.A.; Birkel, C.S.; Hong, B.C.; Seshadri, R. *Chem. Mater.* **2012**, 24(6), 1198-1204.
- (15) Blasse, G.; Brill, A. *Appl. Phys. Lett.* **1967**, 11, 53.
- (16) Bachmann, V.; Ronda, C.; Meijerink, A. *Chem. Mater.* **2009**, 21, 2077-2084.
- (17) Blasse, G.; Wanmaker, W.L.; ter Vrugt J.W.; Brill, A. *Philips Res. Repts.* **1968**, 23, 189-200.
- (18) Li, Q.Y.; de With, G.; Hintzen, H.T. *Chem. Mater.* **2005**, 15, 4492-4496.
- (19) Li, Q.Y.; Delsing, A.C.A.; de With, G.; Hintzen, H.T. *Chem. Mater.* **2005**, 17, 3242-3248.
- (20) Li, Q.Y.; van Steen, J.E.J.; van Kreveld, J.W.H.; Botty, G. Delsing, A.C.A.; DiSalvo, F.J.; de With, G.; Hintzen, H.T. *J. Alloys. Comp.* **2006**, 417, 273-279.
- (21) Li, Q.Y.; de With, G.; Hintzen, H.T. *J. Lumin.* **2006**, 116, 107-116.
- (22) Brinkley, S.E.; Pfaff, N.; Denault, K.A.; Hintzen, H.T. (Bert); Seshadri, R.; Nakamura, S.; DenBaars, S. P. *Appl. Phys. Lett.* **2011**, 99, 241106(1-3).



Precursors for Phosphor Materials

For a complete list of available materials, visit aldrich.com/periodic

Name	Composition	Purity	Description	Prod. No.
Magnesium carbonate trihydrate	MgCO ₃ · 3H ₂ O	90%	solid	751782-25G
Magnesium oxide	MgO	99.995% trace metals basis	powder	529699-10G 529699-50G
Magnesium oxide	MgO	-	nanopowder, particle size <50 nm (BET)	549649-5G 549649-25G
Aluminum nitride	AlN	99.8% trace metals basis	powder, -200 mesh	756393-5G
Aluminum cerium oxide	AlCeO ₃	99% trace metals basis	nanopowder, particle size <50 nm (BET)	637866-10G 637866-50G
Aluminum oxide	Al ₂ O ₃	20 wt. % in H ₂ O	particle size <50 nm (TEM)	642991-100ML
Aluminum oxide	Al ₂ O ₃	20 wt. % in isopropanol	nanoparticles, particle size <50 nm (DLS)	702129-100G 702129-500G
Aluminum isopropoxide	Al[OCH(CH ₃) ₂] ₃	≥99.99% trace metals basis	powder and chunks	229407-10G 229407-50G 229407-250G
Aluminum oxide	Al ₂ O ₃	-	nanopowder, particle size <50 nm (TEM)	544833-10G 544833-50G
Aluminum oxide	Al ₂ O ₃	≥99%	fused, 200 - 325 mesh	342661-1KG
Aluminum oxide	Al ₂ O ₃	-	calcined powder, 150 - 325 mesh	342726-100G
Aluminum oxide	Al ₂ O ₃	≥99%	fused powder, 100 - 200 mesh	342653-100G 342653-1KG
Aluminum chloride, anhydrous	AlCl ₃	99.999% trace metals basis	powder	563919-5G 563919-25G
Aluminum silicate	3Al ₂ O ₃ · 2SiO ₂	-	powder	520179-250G
Silicon dioxide, alumina doped	(SiO ₂) _x (Al ₂ O ₃) _y , aluminum 7.5 wt. %	99.99% trace metals basis, 20 wt. % in H ₂ O	dispersion nanoparticles, particle size <50 nm	701491-25ML 701491-100ML
Silicon dioxide	SiO ₂	99.5% trace metals basis	nanopowder, particle size 10 - 20 nm (SAXS)	637238-50G 637238-250G 637238-500G
Silicon dioxide	SiO ₂	≥99.995% trace metals basis	powder	204358-5G 204358-20G 204358-100G
Silicon monoxide	SiO	-	powder, -325 mesh	262951-50G 262951-250G
Silicon monoxide	SiO	99.99% trace metals basis	pieces, 3 - 10 mm	336823-100G
Calcium nitride	Ca ₃ N ₂	99% trace metals basis (contains <0.5% Mg)	powder, -200 mesh	756415-5G
Calcium iodide hydrate	CaI ₂ · xH ₂ O	99.995% trace metals basis	solid	751979-5G
Calcium carbonate	CaCO ₃	≥99.999% trace metals basis	powder	481807-5G 481807-25G
Calcium chloride, anhydrous	CaCl ₂	99.99% trace metals basis	powder	499609-1G 499609-10G
Calcium oxide, anhydrous	CaO	≥99.99% trace metals basis	powder	451711-5G 451711-25G
Calcium silicate	CaSiO ₃	99%	-200 mesh	372668-50G 372668-250G
Germanium(IV) oxide	GeO ₂	≥99.99% trace metals basis	powder	483702-5G 483702-25G
Germanium(IV) oxide	GeO ₂	99.999% trace metals basis	powder	483001-10G 483001-50G
Strontium nitride	Sr ₃ N ₂	99.5%	powder, -60 mesh	756423-1G
Strontium aluminate	SrAl ₂ O ₄	99.5% trace metals basis	powder, -100 mesh	755680-25G
Strontium aluminate, europium and dysprosium doped	Sr _{3.84} Eu _{0.06} Dy _{0.10} Al ₁₄ O ₂₅	99% trace metals basis	powder, 300 mesh	756520-25G
Strontium aluminate, europium and dysprosium doped	Sr _{0.95} Eu _{0.02} Dy _{0.03} Al ₂ O ₄	99% trace metals basis	powder, -300 mesh	756539-25G
Strontium silicate aluminate, europium and dysprosium doped	Sr _{2.90} Eu _{0.03} Dy _{0.07} Al ₂ SiO ₁₁	99% trace metals basis	powder, -300 mesh	756547-25G
Strontium acetylacetonate hydrate	[CH ₃ COCH=C(O-)(CH ₃) ₂] ₂ Sr · xH ₂ O	-	powder	704512-5G 704512-25G
Strontium oxide	SrO	99.9% trace metals basis	powder	415138-10G 415138-50G
Strontium acetate	(CH ₃ CO ₂) ₂ Sr	99.995% trace metals basis	powder	437883-5G
Strontium isopropoxide	Sr(OCH(CH ₃) ₂) ₂	99.9% trace metals basis	crystalline powder	440698-5G 440698-25G



Name	Composition	Purity	Description	Prod. No.
Yttrium silicate, cerium-doped	$Y_{1.99}Ce_{0.01}SiO_5, Y_{1.99}Ce_{0.01}SiO_5$	99.99%	solid, avg. part. size <200 nm (APS)	755095-5G
Yttrium aluminum oxide, cerium-doped	$Y_{2.94}Ce_{0.06}Al_3O_{12}$	99.9%	powder, avg. part. size <200 nm (APS)	755109-5G
Yttrium(III) chloride, anhydrous	YCl_3	99.99% trace metals basis	powder	451363-10G 451363-50G
Yttrium oxide, europium doped	$Y_{1.92}Eu_{0.08}O_3$	99% trace metals basis	powder, 4 - 8 μ m	756490-25G
Yttrium aluminum oxide	$Y_3Al_5O_{12}$	99% trace metals basis	nanopowder, particle size <150 nm (TEM)	634638-25G
Yttrium(III) carbonate hydrate	$Y_2(CO_3)_3 \cdot xH_2O$	99.9% trace metals basis	powder	326054-25G
Yttrium(III) nitrate tetrahydrate	$Y(NO_3)_3 \cdot 4H_2O$	99.999% trace metals basis	powder	217239-10G 217239-50G
Yttrium(III) nitrate tetrahydrate	$Y(NO_3)_3 \cdot 4H_2O$	99.99% trace metals basis	powder and chunks	331309-10G 331309-100G
Yttrium(III) oxide	Y_2O_3	99.999% trace metals basis	powder	204927-10G 204927-50G
Yttrium(III) oxide	Y_2O_3	-	nanopowder, particle size <50 nm	544892-25G
Yttrium(III) acetate hydrate	$(CH_3CO_2)_3Y \cdot xH_2O$	99.9% metals basis	powder	326046-50G 326046-250G
Yttrium isopropoxide oxide	$OY_2(OCH(CH_3)_2)_2$	-	powder	379425-5G
Barium magnesium aluminate, europium doped	$Ba_{0.88}Eu_{0.14}MgAl_{10}O_{17}$	99% trace metals basis	powder, 5 - 9 μ m	756512-25G
Barium nitride	Ba_3N_2	99.7% trace metals basis	powder, -20 mesh	756407-1G
Barium carbonate	$BaCO_3$	99.999% trace metals basis	powder and chunks	202711-25G 202711-100G
Barium chloride	$BaCl_2$	99.999% trace metals basis	powder and chunks	202738-5G 202738-25G 202738-100G
Barium oxide	BaO	99.99% trace metals basis	powder	554847-5G 554847-25G
Barium acetate	$(CH_3COO)_2Ba$	99.999% trace metals basis	powder or crystals	255912-10G 255912-50G
Cerium magnesium aluminate, terbium doped	$Ce_{0.83}Tb_{0.37}MgAl_{10}O_{19}$	99%	powder, 4 - 8 μ m	756504-25G
Cerium(IV) oxide	CeO_2	>99.95% trace metals basis	nanopowder, particle size <50 nm (BET)	700290-25G 700290-100G
Cerium(IV) oxide	CeO_2	99.995% trace metals basis	powder	202975-10G 202975-50G
Cerium(IV) oxide, dispersion	CeO_2	10 wt. % in H_2O	dispersion nanoparticles, particle size <25 nm	643009-100ML 643009-250ML
Cerium(III) acetate hydrate	$Ce(CH_3CO_2)_3 \cdot xH_2O$	99.99% trace metals basis	powder or crystals	529559-10G
Europium(II) bromide	$EuBr_2$	99.99% trace metals basis	powder	751936-1G
Europium(III) oxide	Eu_2O_3	99.5% trace metals basis	nanopowder, particle size <150 nm (TEM)	634298-25G
Europium(III) oxide	Eu_2O_3	99.999% trace metals basis	powder and chunks	323543-1G 323543-5G
Europium(III) acetate hydrate	$Eu(CH_3CO_2)_3 \cdot xH_2O$	99.999% trace metals basis	powder and chunks	545090-1G 545090-10G
Gadolinium(III) oxide	Gd_2O_3	99.8% trace metals basis	nanopowder, particle size <100 nm (BET)	637335-10G 637335-50G
Gadolinium(III) chloride hydrate	$GdCl_3 \cdot xH_2O$	99.99% trace metals basis	solid	450855-10G 450855-50G

Sigma-Aldrich® Worldwide Offices

Argentina

Free Tel: 0810 888 7446
Tel: (+54) 11 4556 1472
Fax: (+54) 11 4552 1698

Australia

Free Tel: 1800 800 097
Free Fax: 1800 800 096
Tel: (+61) 2 9841 0555
Fax: (+61) 2 9841 0500

Austria

Tel: (+43) 1 605 81 10
Fax: (+43) 1 605 81 20

Belgium

Tel: (+32) 3 899 13 01
Fax: (+32) 3 899 13 11

Brazil

Free Tel: 0800 701 7425
Tel: (+55) 11 3732 3100
Fax: (+55) 11 5522 9895

Canada

Free Tel: 1800 565 1400
Free Fax: 1800 265 3858
Tel: (+1) 905 829 9500
Fax: (+1) 905 829 9292

Chile

Tel: (+56) 2 495 7395
Fax: (+56) 2 495 7396

People's Republic of China

Free Tel: 800 819 3336
Tel: (+86) 21 6141 5566
Fax: (+86) 21 6141 5567

Czech Republic

Tel: (+420) 246 003 200
Fax: (+420) 246 003 291

Denmark

Tel: (+45) 43 56 59 00
Fax: (+45) 43 56 59 05

Finland

Tel: (+358) 9 350 9250
Fax: (+358) 9 350 92555

France

Free Tel: 0800 211 408
Free Fax: 0800 031 052
Tel: (+33) 474 82 28 88
Fax: (+33) 474 95 68 08

Germany

Free Tel: 0800 51 55 000
Free Fax: 0800 64 90 000
Tel: (+49) 89 6513 0
Fax: (+49) 89 6513 1169

Hungary

Tel: (+36) 1 235 9055
Fax: (+36) 1 235 9068

India

Telephone

Bangalore: (+91) 80 6621 9400
New Delhi: (+91) 11 4358 8000
Mumbai: (+91) 22 4087 2364
Pune: (+91) 20 4146 4700
Hyderabad: (+91) 40 3067 7450
Kolkata: (+91) 33 4013 8000

Fax

Bangalore: (+91) 80 6621 9550
New Delhi: (+91) 11 4358 8001
Mumbai: (+91) 22 2579 7589
Pune: (+91) 20 4146 4777
Hyderabad: (+91) 40 3067 7451
Kolkata: (+91) 33 4013 8016

Ireland

Free Tel: 1800 200 888
Free Fax: 1800 600 222
Tel: +353 (0) 402 20370
Fax: + 353 (0) 402 20375

Israel

Free Tel: 1 800 70 2222
Tel: (+972) 8 948 4222
Fax: (+972) 8 948 4200

Italy

Free Tel: 800 827 018
Tel: (+39) 02 3341 7310
Fax: (+39) 02 3801 0737

Japan

Tel: (+81) 3 5796 7300
Fax: (+81) 3 5796 7315

Korea

Free Tel: (+82) 80 023 7111
Free Fax: (+82) 80 023 8111
Tel: (+82) 31 329 9000
Fax: (+82) 31 329 9090

Luxembourg

Tel: (+32) 3 899 1301
Fax: (+32) 3 899 1311

Malaysia

Tel: (+60) 3 5635 3321
Fax: (+60) 3 5635 4116

Mexico

Free Tel: 01 800 007 5300
Free Fax: 01 800 712 9920
Tel: (+52) 722 276 1600
Fax: (+52) 722 276 1601

The Netherlands

Tel: (+31) 78 620 5411
Fax: (+31) 78 620 5421

New Zealand

Free Tel: 0800 936 666
Free Fax: 0800 937 777
Tel: (+61) 2 9841 0555
Fax: (+61) 2 9841 0500

Norway

Tel: (+47) 23 17 60 00
Fax: (+47) 23 17 60 10

Poland

Tel: (+48) 61 829 01 00
Fax: (+48) 61 829 01 20

Portugal

Free Tel: 800 202 180
Free Fax: 800 202 178
Tel: (+351) 21 924 2555
Fax: (+351) 21 924 2610

Russia

Tel: (+7) 495 621 5828
Fax: (+7) 495 621 6037

Singapore

Tel: (+65) 6779 1200
Fax: (+65) 6779 1822

Slovakia

Tel: (+421) 255 571 562
Fax: (+421) 255 571 564

South Africa

Free Tel: 0800 1100 75
Free Fax: 0800 1100 79
Tel: (+27) 11 979 1188
Fax: (+27) 11 979 1119

Spain

Free Tel: 900 101 376
Free Fax: 900 102 028
Tel: (+34) 91 661 99 77
Fax: (+34) 91 661 96 42

Sweden

Tel: (+46) 8 742 4200
Fax: (+46) 8 742 4243

Switzerland

Free Tel: 0800 80 00 80
Free Fax: 0800 80 00 81
Tel: (+41) 81 755 2511
Fax: (+41) 81 756 5449

Thailand

Tel: (+66) 2 126 8141
Fax: (+66) 2 126 8080

United Kingdom

Free Tel: 0800 717 181
Free Fax: 0800 378 785
Tel: (+44) 1747 833 000
Fax: (+44) 1747 833 313

United States

Toll-Free: 800 325 3010
Toll-Free Fax: 800 325 5052
Tel: (+1) 314 771 5765
Fax: (+1) 314 771 5757

Vietnam

Tel: (+84) 8 3516 2810
Fax: (+84) 8 6258 4238

Internet

sigma-aldrich.com

Enabling Science to
Improve the Quality of Life

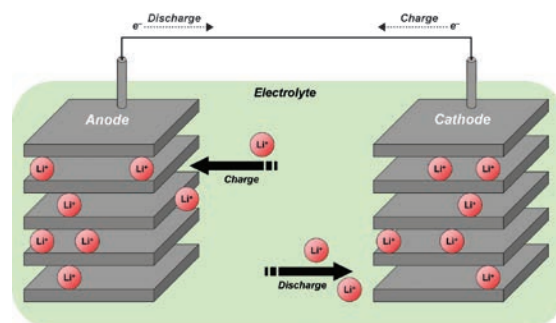
Order/Customer Service (800) 325-3010 • Fax (800) 325-5052
Technical Service (800) 325-5832 • sigma-aldrich.com/techservice
Development/Custom Manufacturing Inquiries **SAFC**® (800) 244-1173
Safety-related Information sigma-aldrich.com/safetycenter

World Headquarters
3050 Spruce St.
St. Louis, MO 63103
(314) 771-5765
sigma-aldrich.com

Advanced Lithium-Ion Battery Materials

Lithium-ion batteries (LIB) are the most popular type of rechargeable batteries used in the portable electronics industry, with one of the best energy densities, no memory effect, and only a slow loss of charge when not in use. Like other batteries, they are constructed from three primary functional components: an anode, cathode and a conductive electrolyte. In rechargeable lithium-ion batteries, monovalent lithium cations migrate to the negative electrode (anode) during charging cycles and to the positive electrode (cathode) during discharge cycles.

Conventional cathode materials generally fall under two structural categories: layered oxides (such as lithium cobalt oxide), or spinels (such as lithium manganese oxide). Anodes are typically fabricated from carbonaceous materials and the electrolyte is a lithium salt in an organic solvent. Aldrich Materials Science offers a wide range of materials for use in lithium-ion batteries including nano and sub-micron powders for fabrication of the next generation battery components.



Recently Introduced Electrode Materials

Name	Synonym	Composition	Description	Prod. No.
Lithium cobalt phosphate	LCP	LiCoPO ₄	99%, particle size < 0.5 μm	725145
Lithium manganese dioxide	LMO	LiMnO ₂	> 99% trace metals basis, particle size < 1 μm	725137
Lithium manganese oxide	LMO	LiMn ₂ O ₄	> 99%, particle size < 0.5 μm	725129
Lithium manganese nickel oxide	LMNO	Li ₂ Mn ₃ NiO ₈	> 99%, particle size < 0.5 μm	725110
Lithium titanate	LTO	Li ₄ Ti ₅ O ₁₂	> 99%, particle size < 100 nm	702277
Yttrium-Nickel alloy	YNi5	YNi ₅	99.9% trace metals basis	693928
Lithium foil	Li	Li	99.9% trace metals basis, thickness × W 0.75 mm × 19 mm	320080

Recently Introduced Electrolyte Materials

Name	Composition	Description	Prod. No.
Lithium tetrachlorogallate	LiGaCl ₄	99.99% trace metals basis, anhydrous, beads, -10 mesh	736317
Lithium perchlorate	LiClO ₄	99.99% trace metals basis, battery grade, dry	634565
Lithium tetrafluoroborate	LiBF ₄	99.998% trace metals basis, anhydrous, powder	451622
Lithium hexafluorophosphate	LiPF ₆	≥99.99% trace metals basis, battery grade	450227
Ethyl methyl carbonate, EMC	(C ₂ H ₅)CO(CH ₃)	99%	754935
Fluoroethylene carbonate, FEC	C ₃ H ₃ FO ₃	99%	757349
3-(Methylsulfonyl)-1-propyne	(CH ₃)SO ₂ (C ₃ H ₃)	95%	718319
Allyl methyl sulfone	(C ₃ H ₅)SO ₂ (CH ₃)	96%	718203

For complete list of LIB materials, visit aldrich.com/lib



Aldrich Material Science Congratulates

Professor Kristi Anseth

Winner of the Inaugural Materials Research Society (MRS) Mid-Career Researcher Award

The Materials Research Society (MRS) Mid-Career Researcher Award, endowed by Aldrich Materials Science, recognizes exceptional achievements in materials research made by mid-career professionals. It is intended to honor an individual between the ages of 40 and 52, who demonstrates notable leadership in the materials area.

The MRS has selected Kristi S. Anseth, University of Colorado, Boulder, to receive the inaugural Mid-Career Researcher Award *“for exceptional achievement at the interface of materials and biology enabling new, functional biomaterials that answer fundamental questions in biology and yield advances in regenerative medicine, stem-cell differentiation, and cancer treatment.”*



About Professor Kristi Anseth

Dr. Anseth is presently a Howard Hughes Medical Institute Investigator and Distinguished Professor of Chemical and Biological Engineering. Her research interests lie at the interface between biology and engineering where she designs new biomaterials for applications in drug delivery and regenerative medicine. Dr. Anseth's research group has published over 200 publications in peer-reviewed journals and presented over 180 invited lectures in the fields of biomaterials and tissue engineering.

aldrich.com/midcareeraward